Journal of Virology

Virology | Full-Length Text

The human cellular protein NoL12 is a specific partner of the HIV-1 nucleocapsid protein NCp7

Sarwat Zgheib,[1] Nedal Taha,[1] Manon Zeiger,[1] Oleksandr Glushonkov,[1] Thiebault Lequeu,[1] Halina Anton,[1] Pascal Didier,[1] Emmanuel Boutant,[1] Yves Mély,[1] Eléonore Réal[1]

AUTHOR AFFILIATION See affiliation list on p. 18.

ABSTRACT The human immunodeficiency virus-1 (HIV-1) nucleocapsid protein (NCp7) is a nucleic acid chaperone protein with two highly conserved zinc fingers. To exert its key roles in the viral cycle, NCp7 interacts with several host proteins. Among them, the human NoL12 protein (hNoL12) was previously identified in genome wide screens as a potential partner of NCp7. hNoL12 is a highly conserved 25 kDa nucleolar RNA-binding protein implicated in the 5′end processing of ribosomal RNA in the nucleolus and thus in the assembly and maturation of ribosomes. In this work, we confirmed the NCp7/hNoL12 interaction in cells by Förster resonance energy transfer visualized by Fluorescence Lifetime Imaging Microscopy and co-immunoprecipitation. The interaction between NCp7 and hNoL12 was found to strongly depend on their both binding to RNA, as shown by the loss of interaction when the cell lysates were pretreated with RNase. Deletion mutants of hNoL12 were tested for their co-immunoprecipitation with NCp7, leading to the identification of the exonuclease domain of hNoL12 as the binding domain for NCp7. Finally, the interaction with hNoL12 was found to be specific of the mature NCp7 and to require NCp7 basic residues.

IMPORTANCE HIV-1 mature nucleocapsid (NCp7) results from the maturation of the Gag precursor in the viral particle and is thus mostly abundant in the first phase of the infection which ends with the genomic viral DNA integration in the cell genome. Most if not all the nucleocapsid partners identified so far are not specific of the mature form. We described here the specific interaction in the nucleolus between NCp7 and the human nucleolar protein 12, a protein implicated in ribosomal RNA maturation and DNA damage response. This interaction takes place in the cell nucleolus, a subcellular compartment where NCp7 accumulates. The absence of binding between hNoL12 and Gag makes hNoL12 one of the few known specific cellular partners of NCp7.

KEYWORDS Human immunodeficiency virus, hNoL12, nucleolus

The human immunodeficiency virus 1 (HIV-1) nucleocapsid protein (NCp7) is a small basic structural protein resulting from the cleavage of the polyprotein Gag by the viral protease during the maturation of the virus particles. The mature NCp7 is composed of 55 amino acids (a.a.) with two highly conserved CCHC type zinc fingers (ZF) bridged by a small basic linker and flanked by unfolded N- and C-terminal basic domains (1–4). NCp7 exhibits nucleic acid (NA) chaperone activity that relies on the formation of a hydrophobic plateau at the top of the two correctly folded ZF (5–9). The capacity of NCp7 to drive specific NA sequences toward their most thermodynamically stable conformation makes it a central player in several steps of the viral life cycle and a potential target for therapies against HIV-1 (10–12). In the early phase, NCp7 was shown to cover the incoming genomic RNA (gRNA) protecting it from cellular nucleases (5, 13, 14). During viral reverse transcription, NCp7 regulates the efficiency and fidelity of primer

Editor Viviana Simon, Icahn School of Medicine at Mount Sinai, New York, New York, USA

Address correspondence to Eléonore Réal, eleonore.real@unistra.fr, or Yves Mély, yves.mely@unistra.fr.

Sarwat Zgheib and Nedal Taha contributed equally to this article. Author order was determined based on co-author agreement and according to the order they were implicated in the project.

The authors declare no conflict of interest.

See the funding table on p. 18.

Received 6 January 2023
Accepted 12 July 2023
Published 11 September 2023

tRNA annealing to the Primer Binding Site on the gRNA and the two obligatory strand transfers (5, 15–18). Moreover, NCp7 is thought to stimulate the viral integration into the host cell genome in the nucleus (5, 19, 20). Interestingly, NCp7 was shown to be released from HIV-1 pseudoparticles during their journey to the nucleus (21), likely as a result of reverse transcription and capsid disassembly (22–25). Moreover, a small sub-population of mature infectious HIV-1 particles only disassemble near the integration sites in the nucleus (26–29), so that NCp7 may be also directly released in the nucleus. In the late phase of infection, NCp7 is found as a domain of the polyprotein Group-specific antigen (Gag) and binds specifically to the genomic encapsidation signal (psi) of the viral RNA, leading to its selective encapsidation into budding virions (30–32).

Among the functions attributed to NCp7, its role in the nucleus of the infected cell is still poorly understood. In fact, the incoming NCp7 is detected as soon as 8 h post infection (p.i.) in the nuclear fraction of CD4-positive HeLa-P4-infected cells (33). It was also detected by immunofluorescence at 10 h p.i. in the nucleus of lymphoblastic H9 cells in which it accumulates till 18 h p.i. (34). Interestingly, after transient overexpression, NCp7 fused to eGFP, mCherry or other fluorescent proteins were found to be distributed all over the cell with a high concentration in the nucleoli (35–37). It is also the case when NCp7 is revealed by immunofluorescence after cell transfection with a plasmid coding for NCp7 (37). The association of NCp7 and the nucleoli was further confirmed by confocal microscopy showing that micro-injected NCp7 labeled by a fluorescent amino acid analog binds preferentially to ribosomal RNA (35, 38).

In this context, in order to decipher the functional role of NCp7 in the nucleus and more specifically in the nucleoli, we searched for a specific nucleolar partner of NCp7 in order to characterize their interaction and its functional consequence on the viral cycle. Several databases of potential partners of the HIV-1 proteins or of proteins functionally implicated in HIV-1 infection of the HIV-1 proteins were published (39–41). Among them, we focused our attention on the human nucleolar protein hNoL12 which was identified as a potential specific NCp7 partner as it was not retrieved with Gag. hNoL12 is a 25 kDa nucleolar RNA-binding protein which possesses several orthologs called Nop25 in *Rattus norvegicus,* Rrp17p in the yeast *Saccharomyces cerevisiae*, and Viriato in Drosophila. Only few data are available on hNoL12 functions in the cells. The first data available on hNoL12 came from a set of studies on Nop25 showing that it harbors several nuclear and nucleolar localization signals (42, 43) and that it plays an important role in the architecture of the nucleolus (44). Most of the functional data are coming from the study of the yeast protein Rrp17p, which has been shown to be a 5′–3′-RNA exonuclease involved in the nucleolar maturation of the 5′ end of the 60S ribosomal RNA subunit. In addition, Rrp17p is thought to participate in the rRNA transport from the nucleoli toward the nuclear membrane making a link between ribosome assembly and transport. Rrp17p knockout is lethal for the yeast and can be rescued by the expression of hNoL12 underlining that the two proteins must share some if not all of their functions (45). A study published in 2017 described hNoL12 as a multifunctional protein, localized in the nucleoli, the nucleoplasm and the cytoplasm. In the nucleoli, hNoL12 is implicated in the separation of large and small subunit rRNA precursors at site 2 (46). hNoL12 also co-localizes with the RNA/DNA helicase Dhx9 and paraspeckles in the nucleoplasm as well as with GW/P-bodies in the cytoplasm. Moreover, its localization at sites of replication stress and DNA damage suggests that hNoL12 may also participate directly in the regulation of DNA repair and/or DNA damage repair signaling (46).

In this work, we showed that (i) hNoL12 is localized in the granular component of the nucleolus of mammalian cells, (ii) hNoL12 interacts with NCp7 in the nucleolus, and (iii) the interaction requires hNoL12 putative exonuclease domain and NCp7 basic residues as well as the binding of both proteins to RNA.

MATERIALS AND METHODS

Mammalian cell culture and plasmids transfection

HeLa cells (ATCC CCL2) as well as HeLa cells stably expressing NCp7-eGFP or eGFP and 293T cells were cultured in Dulbecco's Modified Eagle Medium (Gibco Life Technologies ref 21885) supplemented with 10% fetal bovine serum (FBS, Gibco) and a mixture of penicillin (100 IU/mL) and streptomycin (100 µg/mL) antibiotics (Lonza DE17-602E) at 37°C in a 5% CO_2 atmosphere. Cells were transfected, using jetPEI Polyplus Transfection according to the manufacturer's protocol.

Jurkat cells, clone E6-1 (ATCC TIB-121) were cultured in RPMI-1640 medium (Gibco Life Technologies ref A1049101) supplemented with 10% fetal bovine serum (FBS, Gibco) and a mixture of penicillin (100 IU/mL) and streptomycin (100 µg/mL) antibiotics (Lonza DE17-602E) at 37°C in a 5% CO_2 atmosphere and passaged by dilution every 2–3 days. Cells were transfected, using Viafect (Promega E4981) at a DNA/Viafect ratio of 1/4 according to the manufacturer's protocol.

Plasmids

peGFP plasmid was obtained by the insertion of eGFP cDNA into a pcDNA3.1(+) vector. The plasmid constructs for VSV-G pseudotyped HIV-1 particles, pMD2.G and pULTRA-GFP, were obtained from Addgene. pCMV-dR8.91 was obtained from Pasteur Institute. peGFP-hNoL12 and its deletion mutants were cloned by Gateway cloning from pET52-hNoL12 vector, a generous gift from Dr Oeffinger Marlene (Institut de recherches cliniques de Montreal), using the primers listed in Table S1 into the destination vector peGFP-C1-GW. peGFP-NoLΔ(22–61) was generated by site-directed mutagenesis using Phusion site-directed mutagenesis kit (Thermoscientific, F541) according to the manufacturer's instructions using the primers listed in Table S1.

The mEos2-hNoL12 construct was obtained by replacing the eGFP cDNA in the peGFP-C1-GW vector corresponding to the Gateway cloning version of peGFP-C1 (Clontech) in order to obtain the vector pmEos2-C1-GW. To do so, the mEos2 cDNA was inserted between NheI and XhoI restriction sites of a digested peGFP-C1-GW. The cDNA coding for hNoL12 was thus cloned as described above. The integrity of all plasmid constructs was assessed by DNA sequencing (GATC Biotech, Germany).

To construct pNCp7-mEos2 plasmid, mEos2 cDNA was PCR amplified with primers harboring XhoI and XbaI restriction sites at the 5′- and 3′- termini, respectively. After purification, the PCR product was digested with XhoI and XbaI restriction enzymes and inserted into a pcDNA3.1 Zeo(+) vector digested by XhoI/XbaI and dephosphorylated to give pmEos2-pcDNA3.1 Zeo plasmid. The NCp7 cDNA was PCR amplified with primers harboring EcoRI and XhoI restriction sites. The PCR product was purified and digested by EcoRI and XhoI and inserted in fusion to mEos2 in the corresponding cloning sites of pmEos2-pcDNA3.1 Zeo.

NCp7-Flag construct was done by cloning PCR-amplified NCp7 cDNA into BamHI cloning site in 5′ of a 3xFLAG (Sigma, DYKDHDGDYKDHDIDYKDDDDK) coding sequence into a pcDNA3.1 expression vector.

Immunofluorescence

After fixation, cells were permeabilized with 1% Triton X-100 in phosphate buffered saline, pH 7.4 (PBS) for 10 min at room temperature (RT) and blocked in 1% BSA in PBS (Bovine serum albumin, Euromedex, ref 04–100-811-C) for 1 h before being stained. The cells were subjected to immunofluorescence staining with a rabbit anti-hNoL12 antibody (Bethyl Laboratories A302-733A; dilution 1:250) for 2 h at RT, then washed with 1 × PBS three times and incubated with Alexa 568-labeled anti-rabbit secondary antibody (Thermo Fisher, A11011; dilution 1:1,000) at RT for 1 h. After washing, cells were analyzed by confocal microscopy.

Confocal microscopy

Twenty-four hours before transfection with the plasmids coding for the appropriate proteins, HeLa cells were seeded in 12-well plates on a glass coverslip at a density of 8 × 10^4 cells/well. Twenty-four hours post-transfection, the cells were washed with 1X PBS and fixed with 4% paraformaldehyde in PBS for 15 min at RT. After fixation, cells were washed three times with 1X PBS and mounted on slides using Prolong Gold Antifade Reagent (Invitrogen Reference 36930). Images were acquired with a Leica TC SPE II confocal microscopy using a 63 × 1.4 NA oil immersion objective (HXC PL APO 63×/1.40 OIL CS). The eGFP images were obtained by scanning the cells with a 488-nm laser line and using a 500- to 555-nm band-pass for emission. For the mCherry images, a 561-nm laser line was used with a 570- to 625-nm band-pass. Images were analyzed by Image J software (47).

For live cells imaging, cells were seeded in ibidi 35 mm dishes at a density of 1.5 × 10^5 cells/dish and cultured in complete DMEM medium w/o phenol red (Gibco Life Technologies ref 21885). Twenty-four hours post-transfection, the cells were stained just before imaging with Hoechst (1/2,500) for 20 min at 37°C directly added into the culture medium. After a medium change, cells were imaged by confocal.

For the co-localization analysis, several Regions of Interest containing the cell nucleoli or cell nucleoplasm were selected in each cell and the Pearson's coefficient (*P*) was calculated by using JACoP plug-in (48). The value of Pearson's coefficient reflects the correlation between the pixel fluorescence intensities in both channels. *P* may range from 1 to −1, with 1 standing for complete correlation in the case of perfectly co-localized signals, to −1 for an anti-correlation in the case of mutually excluded localizations. The *P* values near zero indicate no dependency between the two channels. The analysis was performed on a total of 50 cells, with 15–20 analyzed cells per experiment in three independent experiments.

High-resolution microscopy

Super-resolution localization microscopy was performed on a home-built setup based on a Nikon Eclipse Ti microscope with 100 × 1.49 NA oil-immersion objective. Laser lines of 488 nm and 561 nm (Oxxius) were used for excitation of mEos2 and the 405 nm laser was used for the photoconversion. Laser power during the experiments was set to 50 mW for the 561 nm laser resulting in 2 kW.cm^{-2} excitation intensity, and 0.5–120 W.cm^{-2} for the 405 nm laser. Laser lines were co-aligned into a single beam using single-band dichroic mirrors (Semrock). An acousto-optic tunable filter (AOTF; Opto-Electronic) was used to switch between lasers (shutter) and change the laser power. Emission from the sample was spectrally filtered by a multi-band dichroic mirror (405/488/561/635 nm, lasers BrightLine quad-edge super-resolution laser dichroic beamsplitter: Di03-R405/488/561/635-t1-25x36, Semrock) and notch filters (405 nm and 561 nm StopLine single-notch filters: NF03-405E-25 and NF03-561E-25, Semrock), and imaged on an EM-CCD camera from Hamamatsu (ImagEM). An additional lens was used to obtain a final magnification of 150× corresponding to a pixel size of 106.7 nm. Before each experiment the point spread function was optimized, and residual optical aberrations (spherical, coma, etc.) were minimized using adaptive optics (Imagine Optics) with the help of TetraSpek bead. Z-stabilization was ensured by the perfect focus system (PFS, Nikon Eclipse Ti) on the microscope. A stack of 20,000 images of 256 × 256 pixels was acquired and analyzed with the Thunder STORM plug-in in ImageJ (49). The following parameters were used to find and fit the signal of each particle: image filtering—wavelet filter B-Spline, scale:2, order:3; approximate localization of molecules—local maximum [peak intensity threshold: 1.4 × std (Wave.F1), connectivity: 8-neighbourhood]; sub-pixel localization of molecules—integrated Gaussian (fitting radius: 4 px, fitting method: weighted least squares, initial sigma: 1.3 px). Results were filtered by sigma 75 nm < sigma < 250 nm, precision < 25 nm. Drift correction was performed either with fiducial markers (max distance: 100 nm, min marker visibility ratio: 0.15, trajectory smoothing: 0.03) or by cross correlation (number of bins: 15, trajectory

smoothing factor: 0.25). Local density filter was used to remove noise created by isolated localizations (distance radius: 50 nm, minimum number of neighbors: 5).

Fluorescence lifetime imaging microscopy (FLIM)

FLIM measurements were performed using the time-correlated single photon counting approach, on a homemade two-photon excitation scanning microscope based on an Olympus IX70 inverted microscope with an Olympus 60 × 1.2 NA water immersion objective operating in the descanned fluorescence collection mode (50, 51). Two-photon excitation at 900 nm was provided by a mode-locked titanium-sapphire laser (Tsunami, Spectra Physics) or an Insight DeepSee (Spectra Physics) laser. Photons were collected using a set of two filters: a short-pass filter with a cutoff wavelength of 680 nm (F75-680; AHF, Germany) and a band-pass filter of 520 ± 17 nm (F37-520; AHF, Germany). The fluorescence was directed to a fiber-coupled avalanche photodiode (SPCM-AQR-14-FC; PerkinElmer), which was connected to a time-correlated single photon counting module (SPC830, Becker & Hickl, Germany). Typically, the samples were continuously scanned for about 60 s to achieve the appropriate photon statistics in order to reliably analyze the fluorescence decays. Moreover, to reach the Nyquist–Shannon sampling criteria, we carried out FLIM measurements using 20 µm × 20 µm scale and 256 pixels × 256 pixels. Data were analyzed using a commercial software package (SPCImage v2.8; Becker & Hickl, Germany). For Förster resonance energy transfer (FRET) experiments, the FRET efficiency (E) was calculated according to: $E = 1 - (\tau_{DA}/\tau_D)$, where τ_{DA} is the lifetime of the donor (eGFP) in the presence of the acceptor (mCherry) and τ_D is the lifetime of the donor in the absence of the acceptor.

Co-immunoprecipitation (co-IP)

For co-IP of overexpressed proteins, 24 h before transfection or co-transfection with 2 µg of each of the plasmids encoding for the appropriate proteins, 293T cells were seeded in 6-well plates at a concentration of 6×10^5 cells/well. Transfected cells were harvested and lysed after 48 h in the following buffer: Tris-HCl 10 mM pH 7.5, NaCl 150 mM, EDTA 1 mM, and 1% NP40, complete Mini-EDTA free protease inhibitor Cocktail Tablets (Roche). Cell lysates were cleared by centrifugation and the protein concentration was assessed by a Bradford assay. An input fraction (30 µg) was kept to check the protein expression level, and the equivalent of 1.5 mg of lysate was incubated for 2 h at 4°C with 1 µg of anti-Flag antibody (Sigma, F1804) on a rotating wheel. After equilibration, 50 µL of Dynabeads protein A (Life technologies, 10002D) were added and the mixture was incubated for 1 h at 4°C. Beads were washed three times with the lysis buffer, resuspended in Laemmli sample buffer (Bio-Rad, 161–0747), boiled for 5 min, and analyzed by western blot.

Co-IP of endogenous hNoL12 was done as mentioned above with slight modification of the lysis buffer composition: Tris-HCl 50 mM pH 7.5, NaCl 150 mM, EDTA 1 mM, 0.5% NP40, complete Mini-EDTA free protease inhibitor Cocktail Tablets, and Phosphatase Inhibitor Cocktail 2 (Sigma; #P5726). The IP antibody is an anti-eGFP antibody (life technologies A11120). The IP was let overnight at 4°C.

Western blots

Proteins and cell lysates were analyzed by 12% SDS-PAGE gels and transferred onto a polyvinylidene difluoride membrane (Amersham, RPN303F). Membranes were immunoblotted either with an anti-Flag (Sigma, F1804; dilution 1:4,000), an anti-eGFP (Proteintech, 66002–1; dilution 1:10,000) or an anti-GAPDH antibody (Millipore, MAB374; dilution 1:5,000) for 1 h at RT for the IP of overexpressed proteins and overnight at 4°C for the IP of cells stably expressing NCp7-eGFP or eGFP. Membranes were washed with Tris-buffered saline 0.1% Tween 20 (TBS-T) three times for 10 min, and then incubated with secondary antibodies (Promega, WB401B and W402B) conjugated to the horseradish peroxidase (Promega, WB401B and W402B; dilution 1:10,000) for 1 h at RT. After washing the membranes with TBS-T, signals were visualized using a chemioluminescent

ECL system (Amersham, ref 25006264) on an Image Quant LAS 4000 apparatus (GE Healthcare).

Pseudovirus production and quantification

For pseudoviral production, 3×10^6 293 T cells were plated onto 100 mm plastic culture dishes. The next day, cells were co-transfected with 3 µg of pMD2.G, 12 µg of pULTRA-GFP, and 6 µg of pCMV-dR8.91 vectors using Jet PEI. Forty-eight hours post transfection, cell culture supernatants were collected, passed through a 0.45-µm pore PVDF low binding filter (Millipore, SLHV033RS), and concentrated twice on a Vivaspin20 (Sartorius, VS2031). Lentiviral particles were aliquoted and stored at −80°C. Viral stocks were titrated by quantification of p24 viral antigen in the cell supernatants by anti-p24 enzyme-linked immunosorbent assay (ELISA) according to the manufacturer's instructions (Lenti-X p24 Rapid Titer Kit).

Pseudoviral infection and protein knockdown

Twenty-four hours before transfection with 50 nM of control siRNA or hNoL12 siRNA (Dharmacon, LU-015834–00-0002 and L-014330–02) using Dharmafect reagent (Dharmacon, Dharmafect1, T-2001–02), HeLa cells were seeded in 6-well plate at a concentration of 10^5 cells/well. Seventy-two hours post transfection, cells were infected with a viral supernatant containing an amount of particle equivalent to 20 ng of p24/well in a complete DMEM with 8 µg/mL polybrene. After 8 h incubation, the cells supernatant was removed and replaced by virus-free medium. Cells were kept for 48 h before lysis and genomic DNA extraction using Qiagen mini blood kit. In this experiment, AZT (an RT inhibitor) applied at the time of the infection and kept throughout the infection at a 5-µM concentration was used as a positive control.

Quantitative PCR

Quantification of integrated lentivector genome was done by PCR amplifications in Hard-shell PCR plates 384-well thin wall (Bio-Rad, HSP3805) in a total volume of 10 µL using the IQ Sybr Green supermix (Bio-Rad, ref: 1708886). Each condition contained 250 nM primers. Gene expression was normalized to the housekeeping gene GAPDH. Primers for HIV pseudogene insertion were U3For: 5′-AGGGCTACGTAACTCCCAAC-3′ and PsiRev: 5′-AGAGCTCCTCTGGTTTCCCT-3′. Primers specific for GAPDH were GAPDHFor: 5′-TCGACAGTCAGCCGCATCTTCTTT-3′ and GAPDHRev: 5′-ACCAAATCCGTTGACTCCGAC-CTT-3′. Quantitative PCRs were done in a CFX384 real-time system (Bio-Rad), and the results were analyzed with the ΔΔCT method with untreated cells as controls.

RESULTS

hNol12 co-localizes with NCp7 in the granular compartment of the nucleolus

The endogenous hNoL12 protein was detected by immunofluorescence on fixed and permeabilized HeLa cells. We found a strong endogenous hNoL12 signal in the nucleoli and a diffused one all over the cytoplasm (Fig. 1A1). The nucleolar hNoL12 localization is in agreement with the one described for the hNoL12 rat ortholog (Nop25) which was found to be restricted to the nucleolus in COS7 cells (43). In parallel, HeLa cells were transiently transfected with either peGFP-hNoL12 or peGFP and fixed 24 h later. eGFP-hNoL12 was found to be mainly restricted to the nucleolus and the nucleoplasm (Fig. 1A2, compare to eGFP in Fig. 1A3). Two explanations can be given, the first is that hNoL12 overexpression tends to increase the nucleolar localization of hNoL12, the second is that the detection with anti-hNoL12 antibody used for the IF results in a certain amount of background in the cytoplasm. The second hypothesis is supported by the background observed in the western blot (Fig. 4B).

The nucleolus is the most prominent non-membrane enclosed substructure of the nucleus. It is organized in three components which are associated to distinct functions in

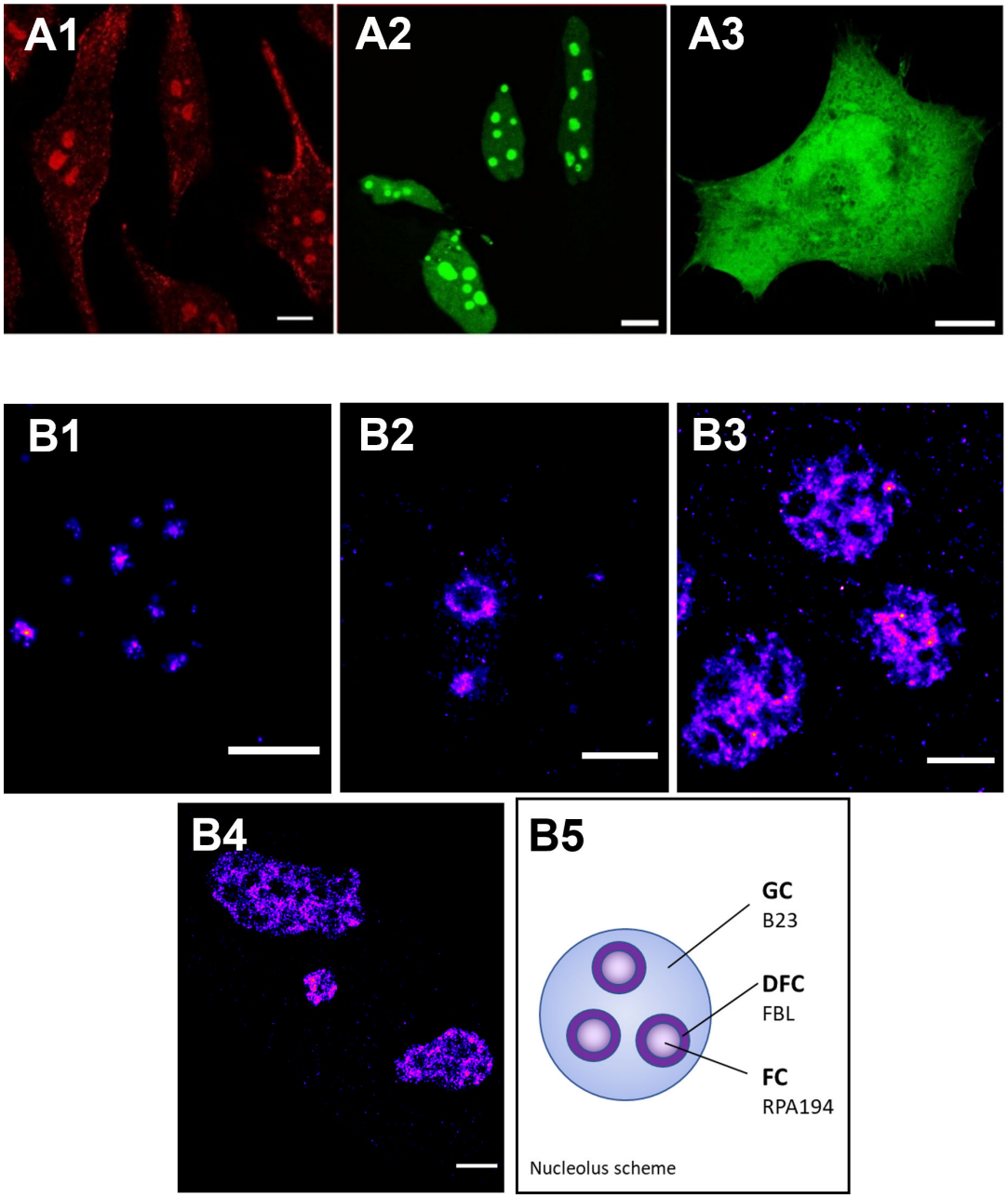

FIG 1 Cellular localization of hNoL12. (A) Intracellular distribution of endogenous hNoL12 (A1), eGFP-hNoL12 (A2), and eGFP (A3). Twenty-four hours after transfection with plasmids coding the labeled proteins, HeLa cells were fixed with PFA and permeabilized to be immunostained with an anti-hNoL12 primary antibody and a secondary antibody coupled to Alexa Fluor 568 as described in Materials and Methods. Cells were imaged using confocal microscopy. The scale bars correspond to 10 µm. (B) PALM imaging of HeLa cells expressing mEos2-RPA194 (B1), mEos2-FBL (B2), mEos2-B23 (B3), mEos2-hNoL12 (B4), and scheme of the nucleolus (B5). Super-resolution images were reconstructed from a 20,000 images stack as described in the "High-resolution microscopy" part of the Materials and Methods section. Scale bars: 2 µm.

rRNA metabolism. Active pol I transcription of rRNA occurs at the interface between the most central regions, the fibrillar centers (FCs) and the dense fibrillar components (DFCs) which surround the FCs. Ribosomal RNA processing starts in the DFC and ends in the granular component (GC) found in the peripheral region of the nucleolus (52).

In a previous work, we demonstrated that the different compartments of the nucleolus can be imaged below the diffraction limit using super resolution localization microscopy (53). Each substructure can be visualized and identified by the independent

expression of specific protein markers fused to the photoactivable mEos2 fluorescent protein. The RNA-polymerase I subunit A (RPA194) is specifically localized in the FC (Fig. 1B1), the DFC is identified by the localization of fibrillarin (FBL, Fig. 1B2), and finally the GC is the site of nucleophosmin also called B23 accumulation (Fig. 1B3). In comparison, hNoL12 (Fig. 1B4) independently expressed as a fusion to mEos2 and imaged by photo-activated localization microscopy (PALM) is mainly localized in the GC subdomain.

To further check that hNoL12 and NCp7 fusion proteins co-localize in the nucleolus, HeLa cells were either transiently transfected with pNCp7-eGFP or co-transfected with pNCp7-mCherry and peGFP-hNoL12 and fixed 24 h later. We observed a strong co-localization of endogenous hNoL12 (Fig. 2A1) and NCp7-eGFP (Fig. 2A2) in the nucleoli (composite image in Fig. 2A3) as well as between overexpressed eGFP-hNoL12 (Fig. 2B1) and NCp7-mCherry (Fig. 2B2 and B3 for composite image). The same co-transfection experiment was done in HeLa cells observed without fixation (see Fig. 2C) and in Jurkat cells imaged after fixation (see Fig. 2D). A co-localization analysis was performed on non-fixed HeLa cells, giving a value of Pearson's coefficient, reflecting the correlation of the two channels, of 0.86 ± 0.11 in nucleoli. This high value indicated a strong positive correlation typical for co-localization of the two proteins. In contrast, the nucleoplasm Pearson's coefficient value was 0.10 ± 0.09, indicating an absence of co-localization.

Thus, our data showed a precise sub-nucleolar localization of hNoL12 in agreement with its probable role in rRNA maturation and its co-localization with NCp7 in several types of cells.

NCp7 interacts with hNoL12 in the nucleoli

Since hNoL12 and NCp7 co-localize in HeLa cell nucleoli, we checked for their direct interaction using FRET-FLIM (Förster Resonance Energy Transfer-Fluorescence Lifetime Imaging Microscopy) technique. HeLa cells were co-transfected with plasmids, coding the two proteins fused to eGFP and mCherry as fluorescence donor and acceptor, respectively. A FRET between eGFP and mCherry only occurs when both fluorophores are less than 10 nm apart, a distance corresponding to intermolecular protein–protein interactions (54, 55). By measuring the fluorescence decay at each pixel of the image, the FLIM technique allows the extraction of the fluorescence lifetime (τ) that, in contrast to fluorescence intensity, does not depend on the instrumentation or the concentration of each fluorophore. In the case of interaction between the two proteins of interest, the energy transfer causes a decrease of the eGFP (donor) fluorescence lifetime. Hence, this technique enables to evidence and map protein–protein interactions within the cell.

As a control, cells expressing eGFP-hNoL12 in the absence of NCp7-mCherry were imaged to determine the mean fluorescence lifetime (τ_m) of eGFP-hNoL12 (Fig. 3A). The fluorescence lifetime, as indicated through a color code in Fig. 3A, is 2.44 ± 0.03 ns, which is very similar to the one of free eGFP (2.39 ± 0.08 ns) (56). Co-expression of eGFP-hNoL12 and NCp7-mCherry resulted in a significant decrease of eGFP fluorescence lifetime, as shown by the color change in Fig. 3B1 with respect to the control in Fig. 3A. This is even more visible when the eGFP-hNoL12 lifetime distribution of all the measured pixels in 11 imaged cells is plotted (Fig. 3C), showing a clearly shifted distribution toward lower lifetime values in the presence of mCherry-labeled NCp7. The average lifetime value in the presence of NCp7-mCherry is 2.15 ± 0.02 ns (Fig. 3B1) giving an average FRET of 12%, a value well above the 5% threshold, required to define a bona fide interaction (55). A more relevant way to analyze the fluorescence decays is to use a two components model which allows taking into account the coexistence of two populations: a free eGFP-hNoL12 and/or a bound one to NCp7-mCherry, being associated with two different fluorescence lifetimes. In this two components model: $F(t)=\alpha_1 e^{-t/\tau 1}+\alpha_2 e^{-t/\tau 2}$, the long-lived lifetime τ_2 is associated with the free eGFP-hNoL12 population and is thus fixed at the lifetime of eGFP-hNoL12 expressed alone (2.44 ns). The short component τ_1 is associated to the bound species undergoing FRET and its value as well as its population α_1 are allowed to float. Using this two components model, we found that 35 ± 2% of the eGFP-hNoL12 proteins (Fig. 3B3) were associated with a lifetime of 1.38 ± 0.07 ns

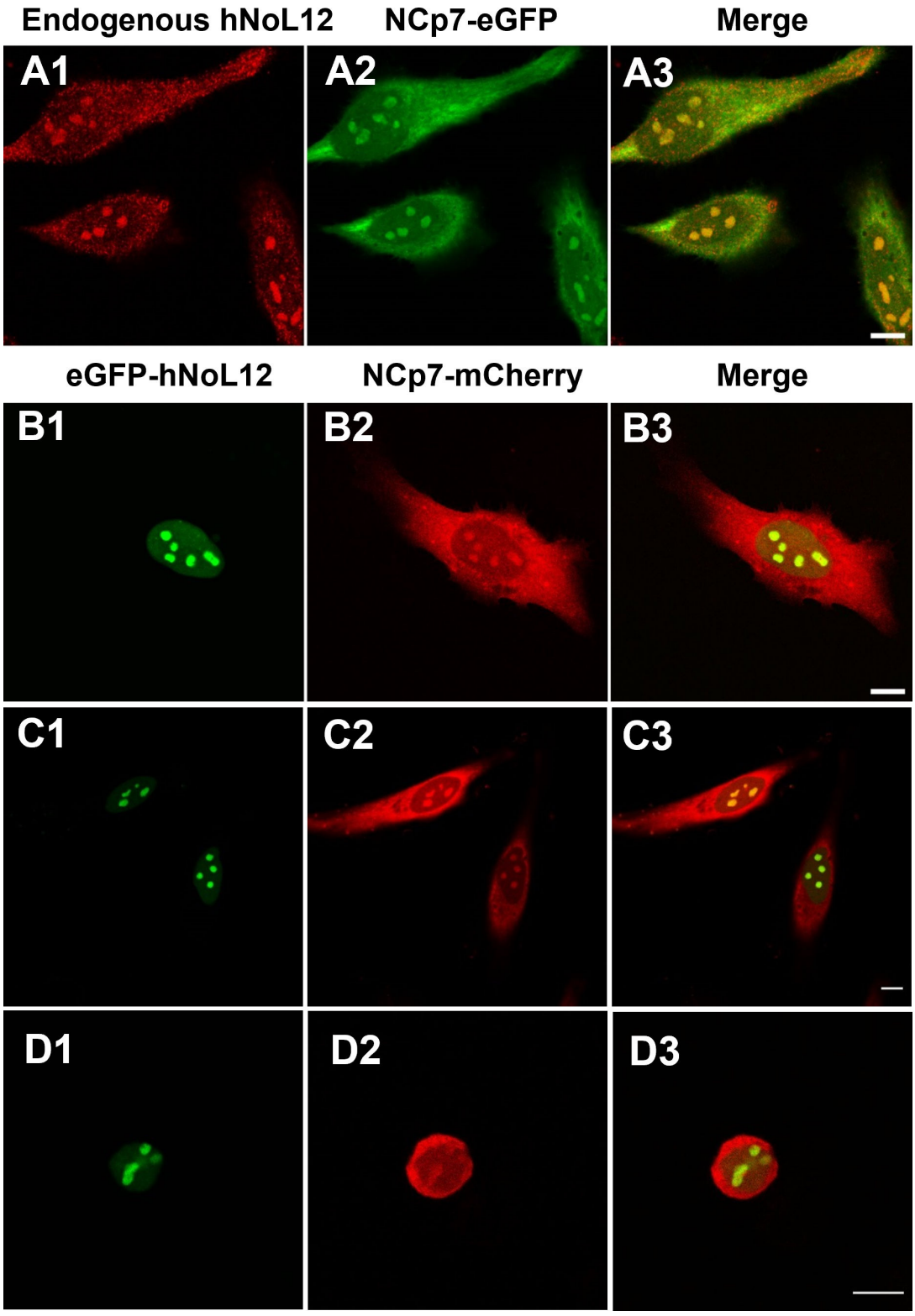

FIG 2 Cellular co-localization of hNoL12 and NCp7. (A) Co-localization in fixed HeLa cells of endogenous hNoL12 (A1) and NCp7-eGFP (A2) and resulting composite image (A3). Co-localization of eGFP-hNoL12 (B1, C1, and D1), NCp7-mCherry (B2, C2, and D2), and resulting composite image (B3, C3, and D3) in fixed HeLa cells (B), living HeLa cells (C), and fixed Jurkat cells (D). HeLa cells and Jurkat cells were fixed with PFA 4% 24 h or 48 h after transfection, respectively (A, B, and D) and in case of panel A permeabilized to be immunostained with an anti-hNoL12 primary antibody and a secondary antibody coupled to Alexa Fluor 568 as described in Materials and Methods. Cells were imaged using confocal microscopy. The scale bars correspond to 10 µm.

and were thus able to FRET with NCp7-mCherry with a high FRET efficiency of 43% indicating a close distance between the fluorescent proteins in the complex (Fig. 3B2). It is noteworthy that the decrease of the eGFP lifetime is particularly important in the nucleoli as indicated by the blue color in the color code in Fig. 3B2. All together, these data clearly demonstrate an interaction between NCp7-mCherry and eGFP-hNoL12 in the cell nuclei and more precisely in the nucleoli.

NCp7-hNoL12 interaction is RNA dependent

In a next step, to confirm the interaction between NCp7 and hNoL12, co-immunoprecipitation experiments (co-IP) were performed on lysates from 293T cells co-transfected with plasmids coding Flag-NCp7 and eGFP-hNoL12 and analyzed by western blot.

The correct expression and detection of Flag-NCp7 (Fig. 4A, lanes 2, 4, and 5), eGFP-hNoL12 (lanes 3 and 4), and eGFP (lane 5) were controlled by western blot using an anti-Flag or an anti-eGFP antibody in parallel to the homogenous loading of the input

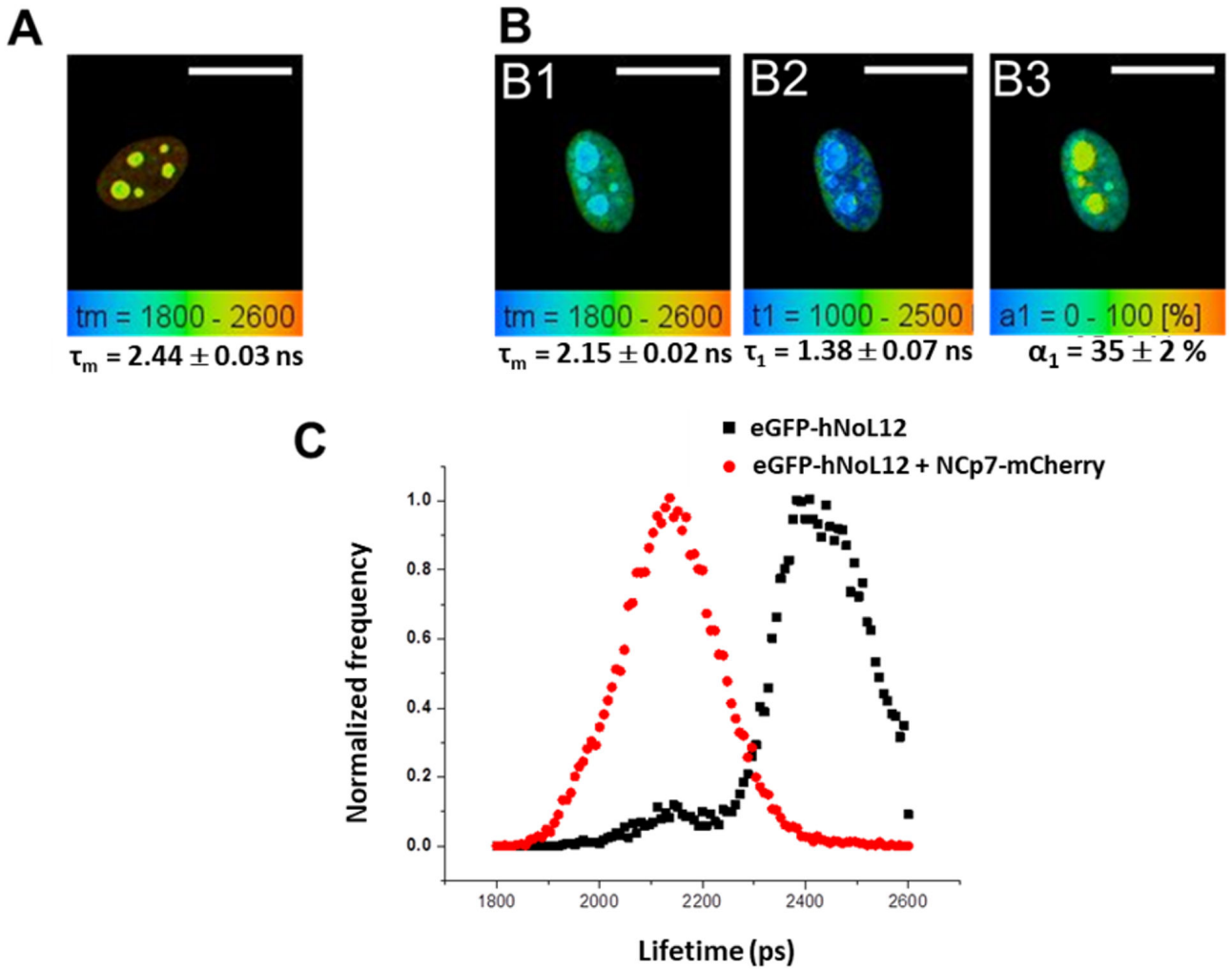

FIG 3 Study of the NCp7/hNoL12 interaction by FRET-FLIM. HeLa cells were transfected by peGFP-hNoL12 without (A) or with pNCp7-mCherry (B). Twenty-four hours post-transfection, the fluorescence decays were measured for each pixel and analyzed using a one- or two-population model. The mean eGFP fluorescence lifetime (τ_m) value of each pixel converted into a color code is given in A and B1 for the one population analysis. In B2 and B3 are given the values of the short-lived lifetime ($\tau 1$) and its amplitude (α_1), when a two-population model was used to treat the data. Scale bars correspond to 1 µm. (C) Normalized distribution of τ_m values, expressed in picoseconds for cells expressing eGFP-hNoL12 in the absence (black) or in the presence of NCp7-mCherry (red). Tau values are given as the mean ± SEM for $N = 11$ cells.

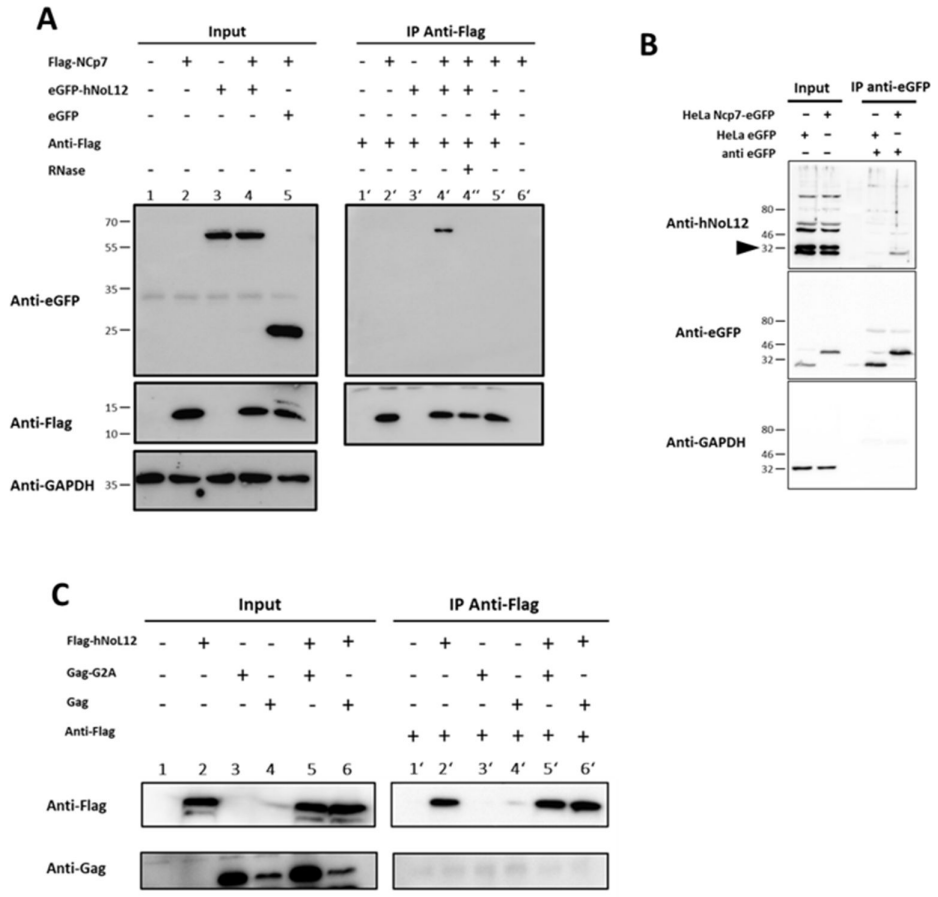

FIG 4 Interaction between hNoL12 and NCp7 or Gag analyzed by co-immunoprecipitation. (A) Lysates of non-transfected 293T cells (lane 1 and 1′) were compared with lysates of cells transfected with pFlag-NCp7 (lane 2 and 2′), peGFP-hNoL12 (3 and 3′), or co-transfected with pFlag-NCp7 and peGFP-hNoL12 (lane 4, 4′, and 4″) or peGFP (lane 5 and 5′). The lysates were loaded on an SDS-PAGE gel before (1 to 5) or after (1′ to 5′) immunoprecipitation with protein A beads linked to an anti-Flag antibody. Lane 6′ represents the lysate used in 2′ incubated with beads without the anti-Flag antibody. After transfer to a nitrocellulose membrane, the presence of each protein is revealed by western blot using the indicated antibodies. (B) Lysates of HeLa cells stably expressing NCp7-eGFP or eGFP were loaded on an SDS-PAGE gel before (Input lanes) or after (IP anti-eGFP lanes) immunoprecipitation with protein A beads linked to an anti-eGFP antibody. After transfer to a nitrocellulose membrane, the presence of each protein is revealed by western blot using the indicated antibodies. In the anti-NoL12 western blot, the specific hNoL12 band is indicated with a black arrow head. (C) Lysates of 293T cells non-transfected (1 and 1′); transfected with pFlag-hNoL12 (2 and 2′); pGag-G2A (3 and 3′); pGag (4 and 4′); and co-transfected with pFlag-hNoL12, pGag-G2A (5 and 5′), or with pFlag-hNoL12 and pGag (6 and 6′) were loaded on an SDS-PAGE gel before (1 to 6) and after (1′ to 6′) immunoprecipitation with protein A beads linked to an anti-Flag antibody. After transfer to a nitrocellulose membrane, the presence of each protein is revealed by western blot using the indicated antibody.

(western-blot anti-GAPDH). The specific Flag-NCp7 immunoprecipitation by an anti-Flag is observed in lanes 2′, 4′, 4″, and 5′ as it does not occur in the absence of an anti-Flag antibody (lane 6′). The eGFP-hNoL12 co-IP is observed only in the presence of Flag-NCp7 (compare lanes 4′ and 3′) and is not due to the eGFP tag as revealed by the absence of eGFP co-IP with Flag-NCp7 (lane 5′). The interaction between Flag-NCp7 and eGFP-hNoL12 is thus confirmed by co-IP. As both NCp7 and hNoL12 interact with NAs and particularly RNAs, a co-IP was also performed from a lysate of cells expressing Flag-NCp7 and eGFP-hNoL12 and treated with RNase. A loss of the NCp7-hNoL12 interaction was observed underlining the RNA-dependent nature of the NCp7/hNoL12 interaction (lane 4″). Taken together, our results demonstrate an RNA-dependent interaction between HIV-1 NCp7 and hNoL12 *in cellulo* after transient overexpression of both proteins in cells.

To verify that NCp7-eGFP interacts with endogenous hNoL12, we used HeLa cell lines stably expressing eGFP or NCp7-eGFP and performed immunoprecipitation using an anti-eGFP. hNoL12 was co-immunoprecipitated from NCp7-eGFP expressing cells but not from the one expressing eGFP (Fig. 4B compares the two "IP anti-eGFP" lanes). The correct expression and detection of NCp7-eGFP, eGFP, and hNoL12 at their correct size were checked in the input lanes. Taken together, these results confirm the specific interaction between endogenous hNoL12 and NCp7.

As NCp7 is also a domain of the polyprotein Gag responsible for the virus budding at the plasma membrane in the late phase of the infection, we also checked by co-IP if Gag and hNoL12 interact. We performed the experiment in HeLa cells overexpressing Gag or GagG2A, the non-myristoylated form of Gag. While Gag is rapidly driven to the cell plasma membrane where hNoL12 is not found, the GagG2A mutant is mostly localized in the cell cytoplasm where the probability to interact with hNoL12 is increased (57–59). As shown in Fig. 4C, neither Gag nor GagG2A was co-immunoprecipitated with an anti-Flag from 293T cells lysates co-expressing Gag or GagG2A and Flag-hNoL12, strongly suggesting that hNoL12 specifically interacts with the mature NCp7 protein.

hNoL12 interactions with NCp7 is mediated through hNoL12 exonuclease domain and NCp7 basic residues

In order to identify the hNoL12 domain responsible for the interaction with NCp7, we constructed hNoL12 deletion mutants which are presented in Fig. 5. We designed these mutants according to the data available on both the rat homolog of hNoL12, Nop25, for which the cellular localizations of several deletion mutants were analyzed and a putative nucleolar localization signal (NoLS) was found (43); and on the yeast ortholog Rrp17p on which a putative exonuclease domain was localized (Fig. S1) (45).

First, we constructed the mutants B to G in fusion to eGFP and tested them for their co-IP with Flag-NCp7 from lysates of 293T cells transfected with plasmids coding hNoL12 mutants in fusion to eGFP and Flag-NCp7. The immunoprecipitates were analyzed by western blot (Fig. 6). We observed, in the input, the correct expression and detection at the appropriate sizes of Flag-NCp7 (lanes 2, 4–10) and all the hNoL12 fragments in fusion to eGFP (lanes 3–10). Flag-NCp7 protein was also specifically immunoprecipitated with an anti-Flag antibody (lane 2′, 4′–10′). As for full-length hNoL12 (lane 4′), the deletion mutants B, C, and D (lane 5′, 6′, and 7′) co-immunoprecipitated with Flag-NCp7, underlining the importance of the hNoL12 N-terminal 96 a.a. in the NCp7/hNoL12 interaction. The co-IP was neither due to an interaction between eGFP and Flag-NCp7 as eGFP was not co-IP with Flag-NCp7 (lane 15′) nor to a binding of eGFP-hNoL12 to the beads (lane 3′). None of the mutants E to G co-immunoprecipitated with Flag-NCp7 (lanes 8′ to 10′), showing that the interaction domain is localized in the first 96 a.a.

To determine more precisely the hNoL12 domain implicated in the interaction with NCp7, we next constructed the mutants H to K fused to eGFP (Fig. 6 lanes 11 to 14 and 11′ to 14′). The mutants I and J co-immunoprecipitated with Flag-NCp7 (lane 12′ and 13′), indicating that the interaction domain could be restricted to the a.a. 22–61, which corresponds to the putative exonuclease domain of hNoL12 (Fig. S1). In parallel, the cellular localization of these mutants (B to K) in living HeLa cells (Fig. S2 and summary in Fig. 5) revealed that the absence of co-IP between NCp7-eGFP and hNoL12 mutants E to H was not due to an inappropriate localization in the cell as all these mutants were found in the nucleoli. In contrast, the absence of nucleolar localization of mutant K could be responsible for the lack of co-IP between this mutant and NCp7-eGFP.

Finally, to confirm the involvement of a.a. 22–61 of hNoL12 in the interaction with NCp7, we constructed two other hNoL12 mutants fused to eGFP. The first one corresponds to hNoL12 deletion of a.a. 22–61 [hNoL12Δ(22–61)] and the second one to the putative interacting domain [hNoL12(22–61)] (respectively, mutant L and M, Fig. 5). As shown in Fig. 7, these mutants were tested for their capacity to co-IP with Flag-NCp7. We observed in the input the correct expression and detection at the expected sizes of both hNoL12 mutants (lanes 4, 5, 7, and 8). After Flag-NCp7 immunoprecipitation using an

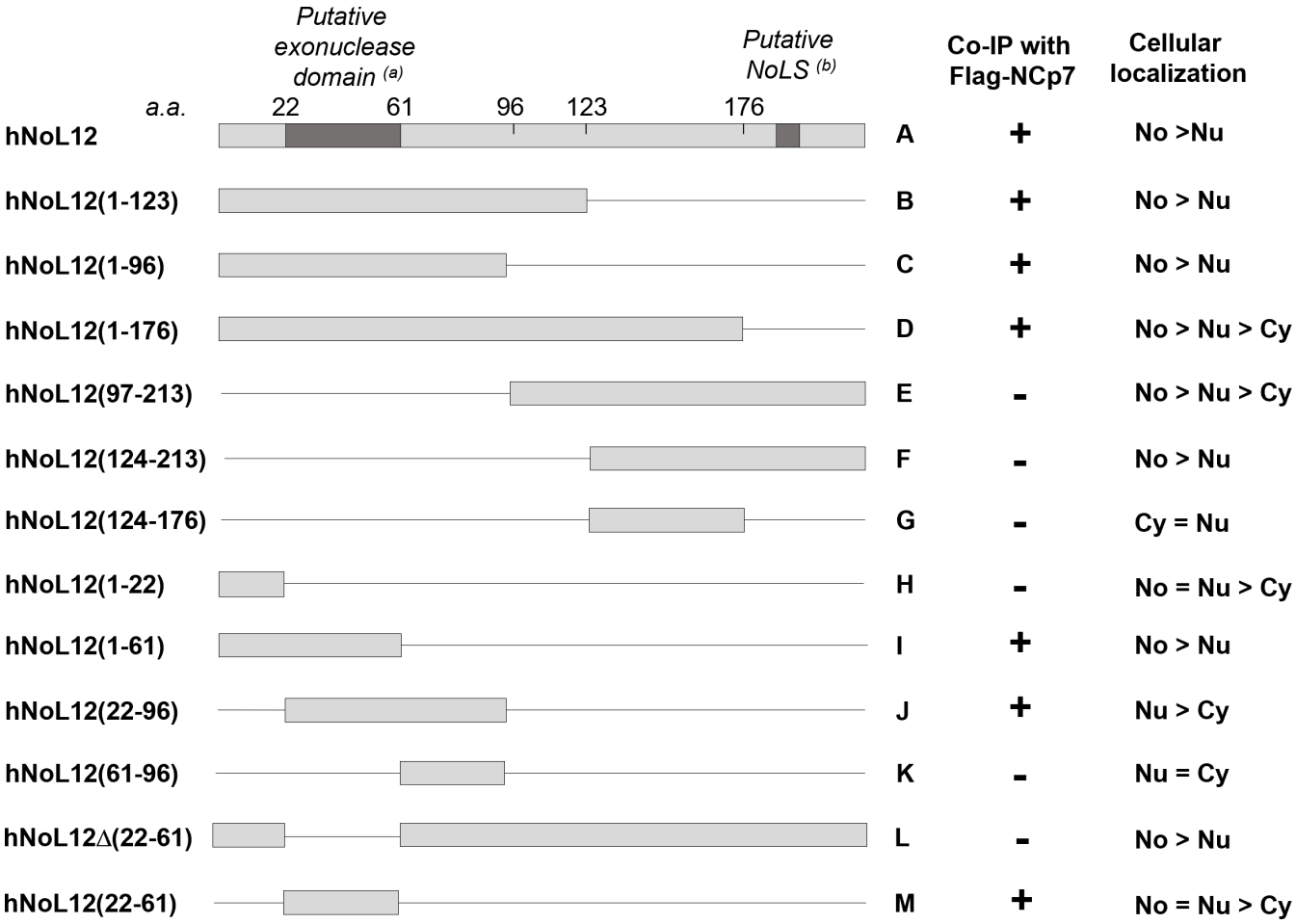

FIG 5 Identification of hNoL12 domains interacting with NCp7. Each hNoL12 deletion mutant was cloned in fusion to the C-terminus of eGFP. The putative exonuclease (A) and NoLS (B) domains were identified by Oeffinger et al. on Rrp17p (45) and Fujiwara et al. on Nop25 (42). The results of the co-IP experiments with Flag-NCp7 using anti-Flag antibody for the IP are shown in the penultimate column. The localization [cytoplasm (Cy), nucleoplasm (No), and nucleolus (Nu)] of each mutant is shown in the last columns according to the observed GFP signals in living HeLa cells expressing the corresponding mutant fused to eGFP after transient transfection (see Fig. S2).

anti-Flag antibody (lanes 2′ and 6′ to 9′), we observed a co-IP of hNoL12(22–61) (lane 7′) but not of hNoL12Δ(22–61) (lane 8′) indicating that a.a. 22 to 61 of hNoL12 are necessary and sufficient for the interaction with NCp7.

From the confocal microscopy study on the different hNoL12 mutants, it seems that hNoL12 possesses at least two NoLS. One is localized between a.a. 21 and 61 (Nter-NoLS) and the second, as suggested from the study on Nop25, is between a.a. 176 and 213 (Cter-NoLS). Both of them are able to target hNoL12 to the nucleolus as observed by the strong nucleolar signals observed for mutants F and M (Fig. 5; Fig. S2). However, another sequence between a.a. 61–96 seems to affect the nucleolar localization driven by the Nter-NoLS as mutants J and K are not found in the nucleolus even if they harbor the Nter-NoLs (Fig. S2).

To identify the NCp7 determinants for binding to Nol12, we tested the ability of two NCp7 mutants to interact with hNoL12. In the first mutant (NCp7 SSHS, Fig. 8A) (60), the six Cysteines of the two zinc fingers were mutated in Serine, which prevents zinc binding and zinc finger folding. In the second mutant (NCp7 5KR-5A), two N-terminal basic residues of NCp7 and three basic residues of the linker region were mutated in Alanine. These two mutants are reported to show a decrease in NA binding and chaperone activities of the protein, and to markedly impact the viral infectivity (8, 61–66). We found that the interaction with hNoL12 was abolished for NCp7 5KR-5A (Fig. 8B) and

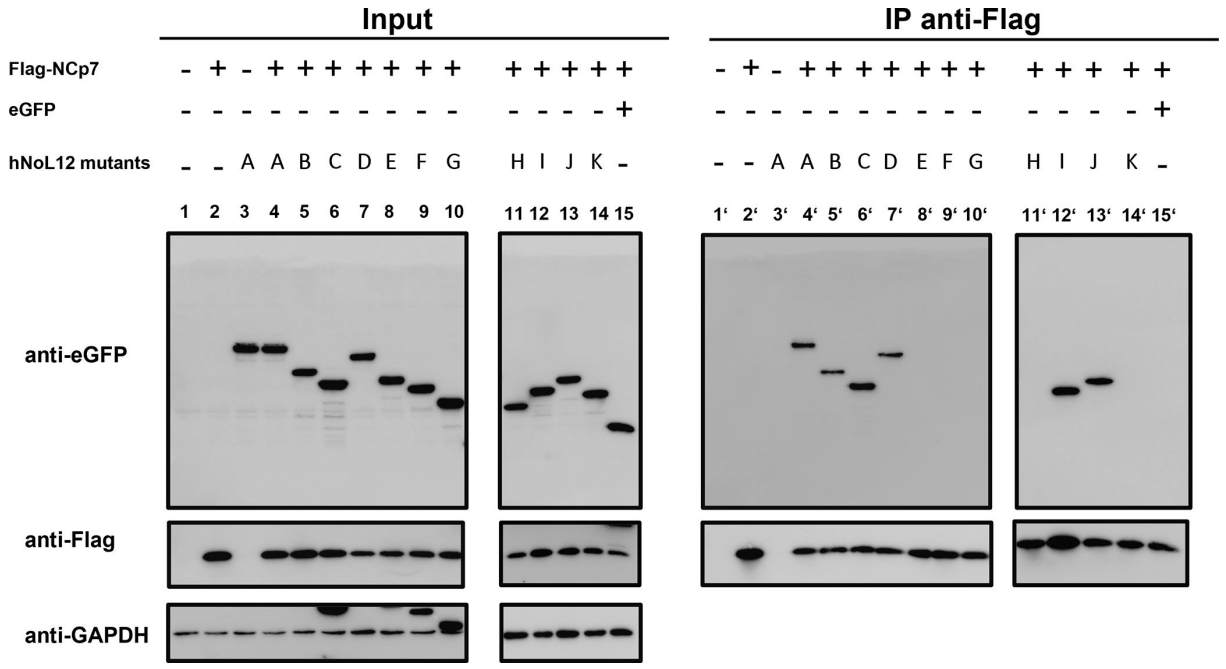

FIG 6 Mapping of the hNoL12 domain interacting with NCp7. Lysates of non-transfected 293T cells (lane 1 and 1′) were compared with lysates of the same cells transfected with pFlag-NCp7 (lane 2 and 2′), peGFP-hNoL12 (3 and 3′), peGFP (15 and 15′), and co-transfected with pFlag-NCp7 and peGFP-hNoL12 (lane 4 and 4′) or peGFP-hNoL12 mutants (lane 5 to 15 and 5′ to 15′). The lysates were loaded on an SDS-PAGE gel before (1 to 15) or after (1′ to 15′) immunoprecipitation with protein A beads loaded with anti-Flag antibody. After transfer to a nitrocellulose membrane, the presence of each protein is revealed by western blot using the mentioned antibodies. GAPDH was used as a loading control.

decreased for NCp7 SSHS (Fig. 8C), indicating that the basic residues of NCp7 are crucial for the interaction with hNoL12 while the folding of the zinc fingers seems somewhat less critical.

Evaluation of the impact of hNoL12 knockdown on the infection by an HIV-1 lentivector

Having validated the interaction between NCp7 and hNoL12 and mapped the interaction domains and determinants, our aim was to test the impact of hNoL12 knockdown on HIV-1 infection. For this purpose, we used a non-replicative lentiviral vector based on HIV-1 as a model of the early stages of infection. The lentivector is pseudotyped with the VSV-G (Vesicular Stomatitis Virus glycoprotein) to enlarge its cellular tropism. An easy way to follow lentiviral infection is to use a pseudovirus with a pseudogenome which encodes for a firefly luciferase (Fluc) gene allowing, after integration in the infected cell genome, the expression under a nonviral promoter of mRNA coding Fluc. However, as hNoL12 is involved in ribosome maturation, its knockdown could have an impact on cell protein synthesis. Therefore, to evaluate the impact of hNoL12 knockdown on HIV-1 infection, we quantified the integrated proviruses in the infected cells. In order to differentiate between actual integrated pseudogenome DNA and plasmids encoding pseudogenome DNA that are potentially transferred from lentivirus-producing cells, we used a lentivirus based on a pULTRA transfer plasmid. In this vector, we can use a couple of primers (U3For and PsiRev) to amplify specifically inserted genomic DNA using the replication of the U3 sequence at the 5′ end of the inserted viral genome during viral reverse transcription (Fig. 9A).

Seventy-two hours after siRNA transfection with either a control siRNA or a siRNA against hNoL12, HeLa cells were infected with the lentiviral vector for 48 h. Genomic DNA was extracted and integrated pseudogenome was quantified by qPCR and normalized to the signal of the housekeeping gene GAPDH. In parallel, in order to control for hNoL12 knockdown, hNoL12 expression levels after siRNA treatment were evaluated by western

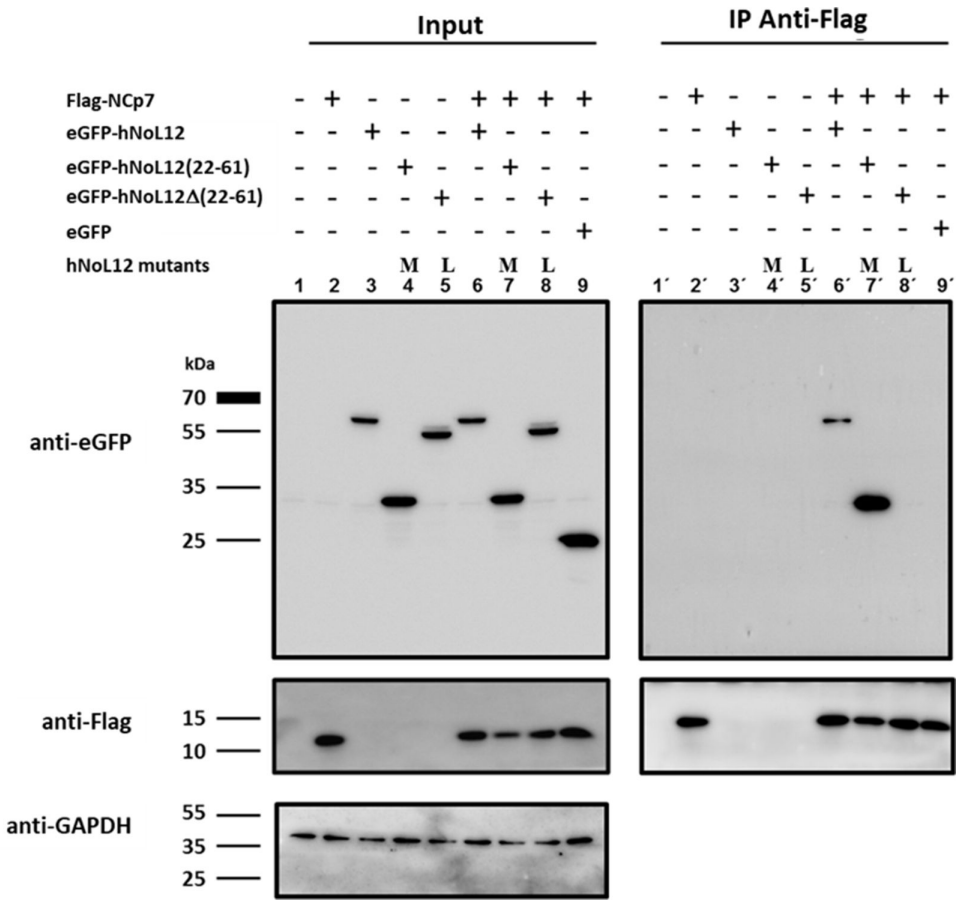

FIG 7 hNoL12 amino acids 22–61 are necessary and sufficient for hNoL12 interaction with NCp7. Lysates of 293T cells transfected or co-transfected with pFlag-NCp7 (lanes 2 and 6 to 9), peGFP-hNoL12 (lanes 3 and 6), peGFP-hNoL12(22–61) (lanes 4 and 7, mutant M in Fig. 5), peGFP-hNoL12Δ22–61 (lanes 5 and 8, mutant L in Fig. 5), or peGFP (lane 9) were submitted to an immunoprecipitation with an anti-Flag antibody (lanes 1′ to 9′). Lysates and immunoprecipitates were loaded on an SDS-PAGE gel, transferred on a nitrocellulose membrane and revealed by western blot using the mentioned antibodies. Lanes 1 and 1′ are the controls with lysates of non-transfected 293T cells. GAPDH was used as a loading control.

blot and normalized to the expression level of GAPDH. The knockdown was observed to reduce hNoL12 expression by about 72% (Fig. 9B). After infection, the normalized level of integrated viral DNA in cells treated with siRNA against hNoL12 (1.12 ± 0.14) was not significantly different from the level in cells treated with control siRNA (1.16 ± 0.25) (Fig. 9C). In contrast, the level of integrated viral DNA was close to zero for infected cells treated with AZT (5 µM, 0.007 ± 0.002), a reverse transcriptase inhibitor used as a positive control. Our data indicate that a partial knockdown of hNoL12 is not able to decrease HeLa cells infection by a pseudotyped non-replicative lentivector.

DISCUSSION

The highly conserved HIV-1 nucleocapsid protein (NCp7) plays key roles in the early steps of HIV-1 replication by notably chaperoning the reverse transcription and integration steps. Interestingly, although productive infection of cells is likely related to a small sub-population of integer viral capsids able to enter into the nucleus (29, 67), NCp7 has been shown to be massively released from viral particles in the cytoplasm of infected cells as a result of reverse transcription and the poor affinity of NCp7 to the double stranded viral DNA as compared to the single stranded gRNA (21). Since each viral particle contains between 1,200 and 5,000 copies of NCp7 (68–72) and since a cell may be simultaneously infected by several viral particles, this suggests that a large number

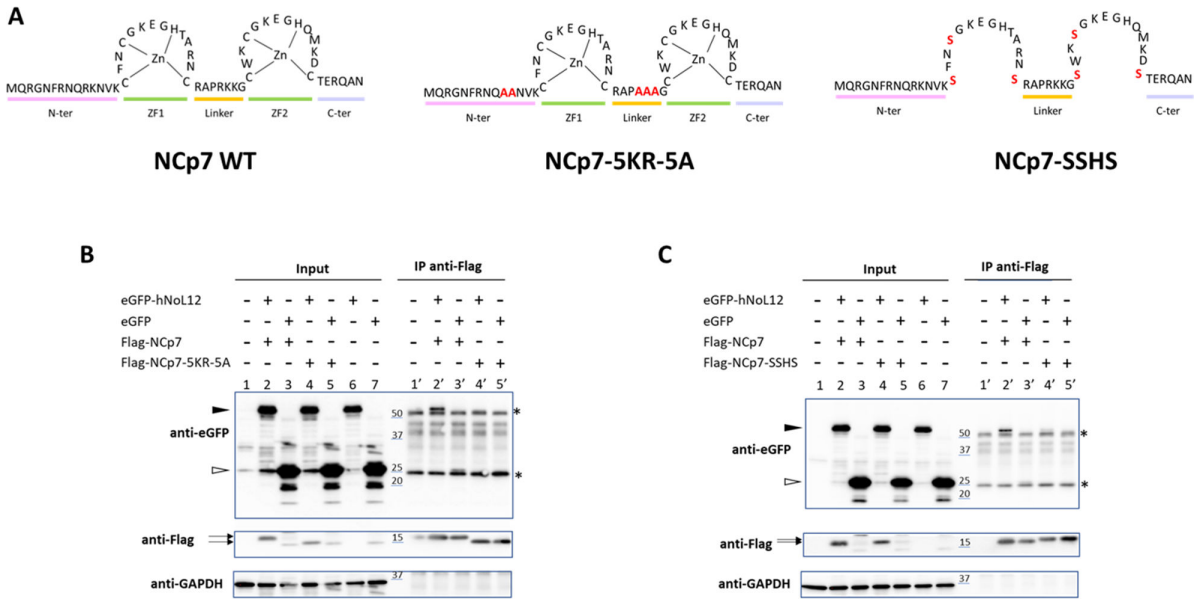

FIG 8 Interaction between hNoL12 and NCp7 mutants analyzed by co-immunoprecipitation. (A) Scheme of NCp7 WT, NCp7 5KR-5A, and NCp7 SSHS mutants. (B) Lysates of non-transfected 293T cells (lane 1 and 1′) were compared with lysates of cells co-transfected with pFlag-NCp7 and peGFP-hNoL12 (lane 2 and 2′) or peGFP (lane 3 and 3′) or pFlag-NCp7-5KR-5A and peGFP-hNoL12 (lane 4 and 4′) or peGFP (lane 5 and 5′) or transfected with peGFP-hNoL12 (lane 6) and peGFP (lane 7). The lysates were loaded on an SDS-PAGE gel before (1 to 7) or after (1′ to 5′) immunoprecipitation with protein A beads linked to an anti-Flag antibody. After transfer to a nitrocellulose membrane, the presence of each protein is revealed by western blot using the indicated antibodies. (C) Lysates of non-transfected 293T cells (lane 1 and 1′) were compared with lysates of cells co-transfected with pFlag-NCp7 and peGFP-hNoL12 (lane 2 and 2′) or peGFP (lane 3 and 3′) or pFlag-NCp7-SSHS and peGFP-hNoL12 (lane 4 and 4′) or peGFP (lane 5 and 5′) or transfected with peGFP-hNoL12 (lane 6) and peGFP (lane 7). The lysates were loaded on an SDS-PAGE gel before (1 to 7) or after (1′ to 5′) immunoprecipitation with protein A beads linked to an anti-Flag antibody. After transfer to a nitrocellulose membrane, the presence of each protein was revealed by western blot using the indicated antibodies. For B and C, eGFP and eGFP-hNoL12 are indicated by white and black arrowheads, respectively, and NCp7 and its mutant with arrows. Stars indicated the detection of heavy (≈ 50 kDa) and light (≈ 25 kDa) chains of the antibody used for the IP.

of NCp7 proteins may be available to interact with host molecular partners and thus additionally contribute to the infection process. Potential host partners of the NCp7 protein have been identified using various screening approaches (39–41).

In this study, we focused on the host nucleolar protein hNoL12 that was suggested to be a selective partner of the mature NCp7 protein. By using FRET-FLIM and co-IP, we unambiguously confirmed the interaction of hNoL12 with the mature NCp7 when both proteins were co-overexpressed or between over-expressed NCp7 and endogenous hNoL12. In contrast, the NC domain-containing HIV-1 polyprotein Gag or a myristoylation defective mutant of Gag known to accumulate in the cytoplasm were not co-immunoprecipitated with Flag-hNoL12 (Fig. 4C). These results suggested that hNoL12 is thus one of the few specific partners of the mature form of the HIV-1 nucleocapsid protein even if we cannot rule out that the interaction between Gag and hNoL12 was undetectable in our experimental conditions. The interaction between NCp7 and hNoL12 was found to strongly depend on their both binding to RNA, as shown by the loss of interaction when the cell lysates were pretreated with RNase. Thus, RNA acts a scaffold to allow the two proteins to stably interact together. Using hNol12 and NCp7 mutants, the interaction between the two proteins was found to be mediated by the exonuclease domain of hNoL12 and the basic residues of NCp7. The folded zinc fingers were shown to also contribute to the interaction. This interaction of NCp7 with hNoL12 is fully consistent with the previously observed accumulation of overexpressed NCp7 in the nucleoli as well as its interaction with 80S ribosomes (35).

In this study, we further showed by PALM imaging that NCp7 preferentially localizes in the nucleolar granular component, a compartment where the rRNAs are assembled with ribosomal proteins (73). The nucleolus plays a key role in ribosome biogenesis and

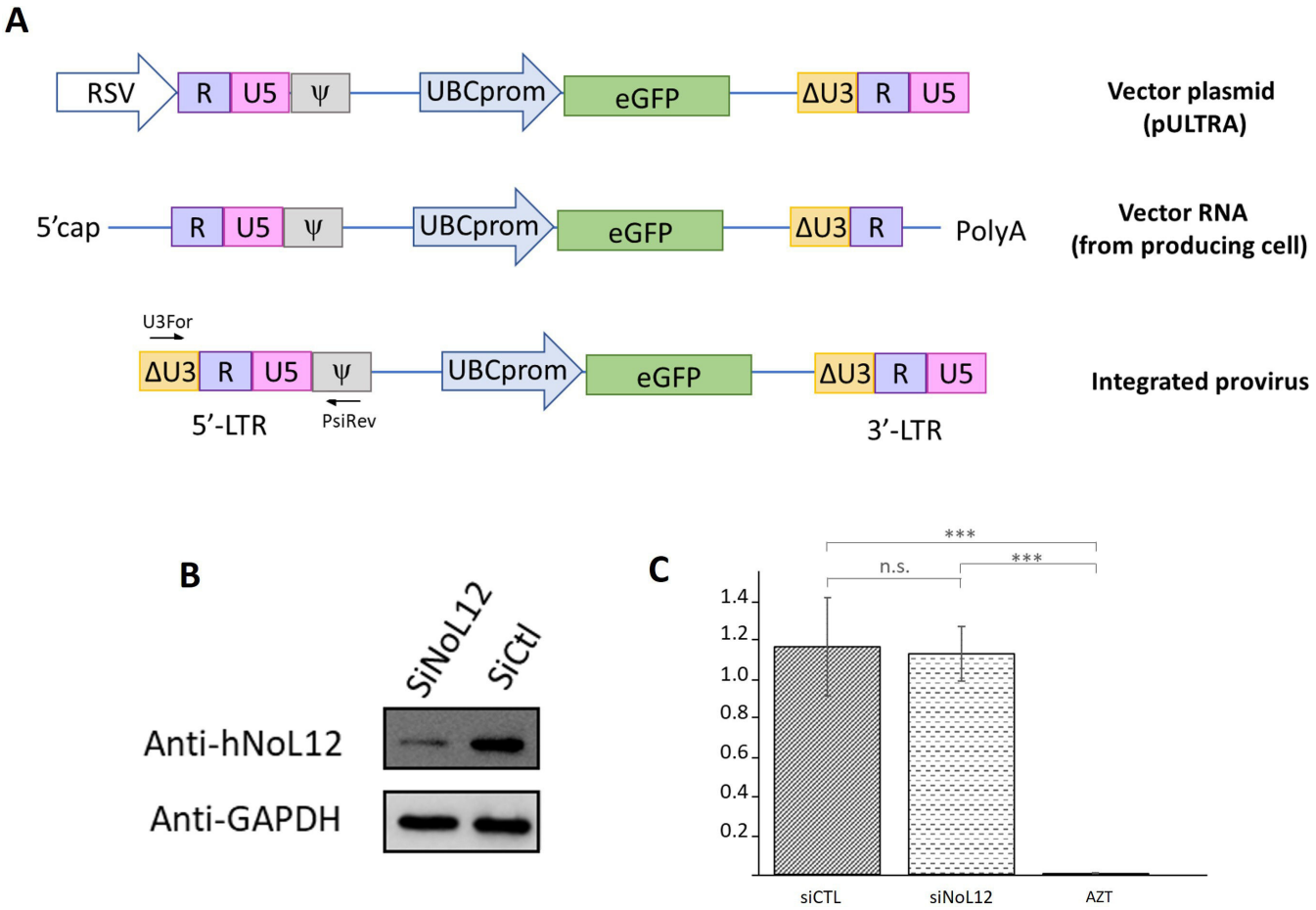

FIG 9 Effect of hNoL12 knockdown on HIV-1 lentiviral vector infection. (A) Scheme of the transfer vector used to quantify provirus integration and localization of the forward and reverse primers for qPCR specific to integrated DNA. (B) Western blot against hNoL12 at 72 h post-transfection of HeLa cells treated with siControl or sihNoL12. GAPDH was used as a loading control. (C) qPCR quantification of provirus integration 48 h post-infection with a lentivirus of HeLa cells previously treated for 72 h with siControl or sihNoL12. The relative quantification was calculated using the ΔΔCt method using the housekeeping gene GAPDH as loading control. AZT (5 µM) was used as a positive control. Data of three independent experiments (*n.s.: non-significant*, ***: $P < 0.001$). Error bars SEM.

numerous cell functions (74), but is also thought to be involved in several viral infections (73, 75–77). The interaction between NCp7 and hNolL2 could have several functional impacts due to hNoL12 implication in rRNA maturation and response to DNA damage and its binding to proteins involved in mRNA metabolism in the nucleus (46).

Similar to its yeast counterpart Rrp17p, hNoL12 is associated with rRNA metabolism and is required for efficient processing at site 2 of the precursors of small and large ribosomal subunits RNA, one of the first step of rRNA maturation in the nucleolus (46, 78). One possibility is that the hNoL12 interaction with NCp7 impacts hNoL12 activity in the process of rRNA maturation. In line with this hypothesis, Kleinman et al. have shown that HIV-1 infection of Jurkat CD4 +T cells leads to the downregulation of genes encoding for proteins involved in the regulation of ribosome biogenesis and especially pre-rRNA processing. In fact, they found that the pre-rRNA 30S obtained after cleavage at site 2 was decreased in infected cells (79). The same defect in site 2 cleavage was observed when hNoL12 expression was knocked down by siRNA (46). In this context, it may be speculated that NCp7 interferes with hNoL12 function in rRNA processing, and thus modifies rRNA production and maturation.

Another interesting partner of hNoL12 is the RNA/DNA helicase Dhx9/RHA, which was found to copurify with hNoL12 in an affinity purification mass spectrometry assay and to co-localize *in vivo* with hNoL12 at replication stress and DNA damage sites (46).

Dhx9/RHA is also known to be incorporated in HIV-1 virion by binding to the primer binding site in the 5′ untranslated region of unspliced and single spliced HIV-1 RNA (80). Moreover, a lower infectivity of Dhx9/RHA defective HIV virions was attributed to a decreased reverse transcription processivity while DHxA/RHA was identified as a processivity factor of HIV-1, increasing the rate of (-)cDNA synthesis (81). Noteworthy, NCp7 ability to increase HIV-1 reverse transcription was linked to its nucleic acids chaperone activity (82), and notably to its ability to unwind G-quadruplexes (83–85). In parallel, Dhx9/RHA was shown to be implicated in the resolution of aberrant DNA and RNA structures including G-quadruplexes, D- and R-loops preventing genomic instability (86–88). It is thus possible that the hNoL12/NCp7 interaction engages the hNoL12/DHx9 complex in the regulation of HIV-1 reverse transcription. NCp7 would thus benefit of this association by increasing its NA chaperone activity as it was already proposed for Gag (89).

Taken together, our data clearly showed that hNoL12 is a specific partner of the mature form of HIV-1 nucleocapsid even if the functional implication of this interaction is still to be determined as no impact on a model of HIV-1 infection by a non-replicating lentivirus was observed in our hands. As only few data are available on hNoL12 functions, its interaction with NCp7 raises, as shown in this discussion, a number of unanswered questions. The determination of NCp7 impact on rRNA maturation profile and ribosome production as well as the study of the functional impact of this interaction in reverse transcription and integration processes would be good tasks to begin with.

ACKNOWLEDGMENTS

We thank members of the Mely lab as well as Daniel D. Scott and Marlene Oeffinger from IRCM. Sarwat Zgheib was supported by a doctoral fellowship from the French Ministère de l'Enseignement Supérieur et de la Recherche. Y.M. is grateful to the Institut Universitaire de France (IUF) for support and providing additional time to be dedicated to research.

AUTHOR AFFILIATION

[1]CNRS, Laboratoire de Bioimagerie et Pathologies - LBP, Université de Strasbourg, Faculté de Pharmacie, Illkirch, France

PRESENT ADDRESS

Sarwat Zgheib, Nouvel Hôpital civil, Centre d'investigation clinique, Strasbourg, France
Nedal Taha, American Red Cross-HLA laboratory, Dedham, Massachusetts, USA
Oleksandr Glushonkov, CNRS, Institut de Biologie Structurale, Université Grenoble, Alpes Grenoble, France

AUTHOR ORCIDs

Yves Mély http://orcid.org/0000-0001-7328-8269
Eléonore Réal http://orcid.org/0000-0002-5523-4408

FUNDING

Funder	Grant(s)	Author(s)
Ministère de l'Education Nationale, de l'Enseignement Superieur et de la Recherche (MESR)		Sarwat Zgheib
Institut Universitaire de France (IUF)		Yves Mély

AUTHOR CONTRIBUTIONS

Sarwat Zgheib, Conceptualization, Data curation, Formal analysis, Investigation, Writing – original draft | Nedal Taha, Data curation, Formal analysis, Investigation | Manon Zeiger, Data curation, Investigation | Oleksandr Glushonkov, Data curation, Formal analysis, Investigation | Thiebault Lequeu, Investigation | Halina Anton, Data curation, Formal analysis, Writing – review and editing | Pascal Didier, Formal analysis, Writing – review and editing | Emmanuel Boutant, Methodology, Writing – review and editing | Yves Mély, Funding acquisition, Supervision, Validation, Writing – review and editing | Eléonore Réal, Conceptualization, Data curation, Formal analysis, Methodology, Project administration, Supervision, Validation, Writing – original draft, Writing – review and editing

ADDITIONAL FILES

The following material is available online.

Supplemental Material

Supplemental figures and table (JVI00040-23-s0001.pdf). Table S1 and Fig. S1 and S2.

REFERENCES

1. Summers MF, South TL, Kim B, Hare DR. 1990. High-resolution structure of an HIV zinc fingerlike domain via a new NMR-based distance geometry approach. Biochemistry 29:329–340. https://doi.org/10.1021/bi00454a005
2. Summers MF, Henderson LE, Chance MR, Bess JW, South TL, Blake PR, Sagi I, Perez-Alvarado G, Sowder RC, Hare DR. 1992. Nucleocapsid zinc fingers detected in retroviruses: EXAFS studies of intact viruses and the solution-state structure of the nucleocapsid protein from HIV-1. Protein Sci 1:563–574. https://doi.org/10.1002/pro.5560010502
3. Morellet N, Jullian N, De Rocquigny H, Maigret B, Darlix JL, Roques BP. 1992. Determination of the structure of the nucleocapsid protein NCp7 from the human immunodeficiency virus type 1 by 1H NMR. EMBO J 11:3059–3065. https://doi.org/10.1002/j.1460-2075.1992.tb05377.x
4. Lee BM, De Guzman RN, Turner BG, Tjandra N, Summers MF. 1998. Dynamical behavior of the HIV-1 nucleocapsid protein. J Mol Biol 279:633–649. https://doi.org/10.1006/jmbi.1998.1766
5. Darlix J-L, Godet J, Ivanyi-Nagy R, Fossé P, Mauffret O, Mély Y. 2011. Flexible nature and specific functions of the HIV-1 nucleocapsid protein. J Mol Biol 410:565–581. https://doi.org/10.1016/j.jmb.2011.03.037
6. Bourbigot S, Ramalanjaona N, Boudier C, Salgado GFJ, Roques BP, Mély Y, Bouaziz S, Morellet N. 2008. How the HIV-1 nucleocapsid protein binds and destabilises the (–)primer binding site during reverse transcription. J Mol Biol 383:1112–1128. https://doi.org/10.1016/j.jmb.2008.08.046
7. De Guzman RN, Wu ZR, Stalling CC, Pappalardo L, Borer PN, Summers MF. 1998. Structure of the HIV-1 nucleocapsid protein bound to the SL3 Ψ-RNA recognition element. Science 279:384–388. https://doi.org/10.1126/science.279.5349.384
8. Wu H, Mitra M, Naufer MN, McCauley MJ, Gorelick RJ, Rouzina I, Musier-Forsyth K, Williams MC. 2014. Differential contribution of basic residues to HIV-1 nucleocapsid protein's nucleic acid chaperone function and retroviral replication. Nucleic Acids Res 42:2525–2537. https://doi.org/10.1093/nar/gkt1227
9. Cosa G, Harbron EJ, Zeng Y, Liu H-W, O'Connor DB, Eta-Hosokawa C, Musier-Forsyth K, Barbara PF. 2004. Secondary structure and secondary structure dynamics of DNA hairpins complexed with HIV-1 NC protein. Biophys J 87:2759–2767. https://doi.org/10.1529/biophysj.104.043083
10. Mori M, Kovalenko L, Lyonnais S, Antaki D, Torbett BE, Botta M, Mirambeau G, Mély Y. 2015. Nucleocapsid protein: a desirable target for future therapies against HIV-1, p 53–92. In Torbett BE, DS Goodsell, DD Richman (ed), The future of HIV-1 therapeutics. Springer International Publishing, Cham. https://doi.org/10.1007/978-3-319-18518-7
11. Sancineto L, Iraci N, Tabarrini O, Santi C. 2018. NCp7: targeting a multitasking protein for next-generation anti-HIV drug development part 1: covalent inhibitors. Drug Discov Today 23:260–271. https://doi.org/10.1016/j.drudis.2017.10.017
12. Iraci N, Tabarrini O, Santi C, Sancineto L. 2018. NCp7: targeting a multitask protein for next-generation anti-HIV drug development part 2. Noncovalent inhibitors and nucleic acid binders. Drug Discov Today 23:687–695. https://doi.org/10.1016/j.drudis.2018.01.022
13. Thomas JA, Gorelick RJ. 2008. Nucleocapsid protein function in early infection processes. Virus Res 134:39–63. https://doi.org/10.1016/j.virusres.2007.12.006
14. Darlix J-L, de Rocquigny H, Mauffret O, Mély Y. 2014. Retrospective on the all-in-one retroviral nucleocapsid protein. Virus Res 193:2–15. https://doi.org/10.1016/j.virusres.2014.05.011
15. Kim J, Roberts A, Yuan H, Xiong Y, Anderson KS. 2012. Nucleocapsid protein annealing of a primer-template enhances (+)-strand DNA synthesis and fidelity by HIV-1 reverse transcriptase. J Mol Biol 415:866–880. https://doi.org/10.1016/j.jmb.2011.12.034
16. Saadatmand J, Kleiman L. 2012. Aspects of HIV-1 assembly that promote primer tRNA(Lys3) annealing to viral RNA. Virus Res 169:340–348. https://doi.org/10.1016/j.virusres.2012.06.001
17. Stewart-Maynard KM, Cruceanu M, Wang F, Vo M-N, Gorelick RJ, Williams MC, Rouzina I, Musier-Forsyth K. 2008. Retroviral nucleocapsid proteins display nonequivalent levels of nucleic acid chaperone activity. J Virol 82:10129–10142. https://doi.org/10.1128/JVI.01169-08
18. Hargittai MRS, Gorelick RJ, Rouzina I, Musier-Forsyth K. 2004. Mechanistic insights into the kinetics of HIV-1 nucleocapsid protein-facilitated tRNA annealing to the primer binding site. J Mol Biol 337:951–968. https://doi.org/10.1016/j.jmb.2004.01.054
19. Carteau S, Gorelick RJ, Bushman FD. 1999. Coupled integration of human immunodeficiency virus type 1 cDNA ends by purified integrase *in vitro*: stimulation by the viral nucleocapsid protein. J Virol 73:6670–6679. https://doi.org/10.1128/JVI.73.8.6670-6679.1999
20. Thomas JA, Gagliardi TD, Alvord WG, Lubomirski M, Bosche WJ, Gorelick RJ. 2006. Human immunodeficiency virus type 1 nucleocapsid zinc-finger mutations cause defects in reverse transcription and integration. Virology 353:41–51. https://doi.org/10.1016/j.virol.2006.05.014
21. Zgheib S, Lysova I, Réal E, Dukhno O, Vauchelles R, Pires M, Anton H, Mély Y. 2019. Quantitative monitoring of the cytoplasmic release of NCp7 proteins from individual HIV-1 viral cores during the early steps of infection. Sci Rep 9:945. https://doi.org/10.1038/s41598-018-37150-0
22. Lyonnais S, Gorelick RJ, Heniche-Boukhalfa F, Bouaziz S, Parissi V, Mouscadet J-F, Restle T, Gatell JM, Le Cam E, Mirambeau G. 2013. A protein ballet around the viral genome orchestrated by HIV-1 reverse transcriptase leads to an architectural switch: from nucleocapsid-condensed RNA to Vpr-bridged DNA. Virus Res 171:287–303. https://doi.org/10.1016/j.virusres.2012.09.008

23. Mukherjee S, Boutant E, Réal E, Mély Y, Anton H. 2021. Imaging viral infection by fluorescence microscopy: focus on HIV-1 early stage. Viruses 13:213. https://doi.org/10.3390/v13020213
24. Dharan A, Campbell EM. 2022. Teaching old dogmas new tricks: recent insights into the nuclear import of HIV-1. Curr Opin Virol 53:101203. https://doi.org/10.1016/j.coviro.2022.101203
25. Aiken C, Rousso I. 2021. The HIV-1 capsid and reverse transcription. Retrovirology 18:29. https://doi.org/10.1186/s12977-021-00566-0
26. Zila V, Margiotta E, Turoňová B, Müller TG, Zimmerli CE, Mattei S, Allegretti M, Börner K, Rada J, Müller B, Lusic M, Kräusslich H-G, Beck M. 2021. Cone-shaped HIV-1 capsids are transported through intact nuclear pores. Cell 184:1032–1046. https://doi.org/10.1016/j.cell.2021.01.025
27. Rouzina I, Bruinsma R. 2014. DNA confinement drives uncoating of the HIV virus. Eur Phys J Spec Top 223:1745–1754. https://doi.org/10.1140/epjst/e2014-02223-x
28. Xu C, Fischer DK, Rankovic S, Li W, Dick RA, Runge B, Zadorozhnyi R, Ahn J, Aiken C, Polenova T, Engelman AN, Ambrose Z, Rousso I, Perilla JR, Campbell EM. 2020. Permeability of the HIV-1 capsid to metabolites modulates viral DNA synthesis. PLoS Biol 18:e3001015. https://doi.org/10.1371/journal.pbio.3001015
29. Burdick RC, Li C, Munshi M, Rawson JMO, Nagashima K, Hu W-S, Pathak VK. 2020. HIV-1 uncoats in the nucleus near sites of integration. Proc Natl Acad Sci U S A 117:5486–5493. https://doi.org/10.1073/pnas.1920631117
30. Dannull J, Surovoy A, Jung G, Moelling K. 1994. Specific binding of HIV-1 nucleocapsid protein to PSI RNA *in vitro* requires N-terminal zinc finger and flanking basic amino acid residues. EMBO J 13:1525–1533. https://doi.org/10.1002/j.1460-2075.1994.tb06414.x
31. Clever J, Sassetti C, Parslow TG. 1995. RNA secondary structure and binding sites for Gag gene products in the 5' packaging signal of human immunodeficiency virus type 1. J Virol 69:2101–2109. https://doi.org/10.1128/JVI.69.4.2101-2109.1995
32. Clever JL, Miranda D, Parslow TG. 2002. RNA structure and packaging signals in the 5' leader region of the human immunodeficiency virus type 1 genome. J Virol 76:12381–12387. https://doi.org/10.1128/jvi.76.23.12381-12387.2002
33. Gallay P, Swingler S, Song J, Bushman F, Trono D. 1995. HIV nuclear import is governed by the phosphotyrosine-mediated binding of matrix to the core domain of integrase. Cell 83:569–576. https://doi.org/10.1016/0092-8674(95)90097-7
34. Zhang J, Crumpacker CS. 2002. Human immunodeficiency virus type 1 nucleocapsid protein nuclear localization mediates early viral mRNA expression. J Virol 76:10444–10454. https://doi.org/10.1128/jvi.76.20.10444-10454.2002
35. Anton H, Taha N, Boutant E, Richert L, Khatter H, Klaholz B, Rondé P, Réal E, de Rocquigny H, Mély Y. 2015. Investigating the cellular distribution and interactions of HIV-1 nucleocapsid protein by quantitative fluorescence microscopy. PLoS One 10:e0116921. https://doi.org/10.1371/journal.pone.0116921
36. Lochmann TL, Bann DV, Ryan EP, Beyer AR, Mao A, Cochrane A, Parent LJ. 2013. NC-mediated nucleolar localization of retroviral Gag proteins. Virus Res 171:304–318. https://doi.org/10.1016/j.virusres.2012.09.011
37. Yu KL, Lee SH, Lee ES, You JC. 2016. HIV-1 nucleocapsid protein localizes efficiently to the nucleus and nucleolus. Virology 492:204–212. https://doi.org/10.1016/j.virol.2016.03.002
38. Sholokh M, Zamotaiev OM, Das R, Postupalenko VY, Richert L, Dujardin D, Zaporozhets OA, Pivovarenko VG, Klymchenko AS, Mély Y. 2015. Fluorescent amino acid undergoing excited state intramolecular proton transfer for site-specific probing and imaging of peptide interactions. J Phys Chem B 119:2585–2595. https://doi.org/10.1021/jp508748e
39. Jäger S, Cimermancic P, Gulbahce N, Johnson JR, McGovern KE, Clarke SC, Shales M, Mercenne G, Pache L, Li K, Hernandez H, Jang GM, Roth SL, Akiva E, Marlett J, Stephens M, D'Orso I, Fernandes J, Fahey M, Mahon C, O'Donoghue AJ, Todorovic A, Morris JH, Maltby DA, Alber T, Cagney G, Bushman FD, Young JA, Chanda SK, Sundquist WI, Kortemme T, Hernandez RD, Craik CS, Burlingame A, Sali A, Frankel AD, Krogan NJ. 2011. Global landscape of HIV-human protein complexes. Nature 481:365–370. https://doi.org/10.1038/nature10719
40. Yeung ML, Houzet L, Yedavalli V, Jeang K-T. 2009. A genome-wide short hairpin RNA screening of jurkat T-cells for human proteins contributing to productive HIV-1 replication. J Biol Chem 284:19463–19473. https://doi.org/10.1074/jbc.M109.010033
41. König R, Zhou Y, Elleder D, Diamond TL, Bonamy GMC, Irelan JT, Chiang C-Y, Tu BP, De Jesus PD, Lilley CE, Seidel S, Opaluch AM, Caldwell JS, Weitzman MD, Kuhen KL, Bandyopadhyay S, Ideker T, Orth AP, Miraglia LJ, Bushman FD, Young JA, Chanda SK. 2008. Global analysis of host-pathogen interactions that regulate early-stage HIV-1 replication. Cell 135:49–60. https://doi.org/10.1016/j.cell.2008.07.032
42. Fujiwara T, Suzuki S, Kanno M, Sugiyama H, Takahashi H, Tanaka J. 2006. Mapping a nucleolar targeting sequence of an RNA binding nucleolar protein, Nop25. Exp Cell Res 312:1703–1712. https://doi.org/10.1016/j.yexcr.2006.02.002
43. Suzuki S, Kanno M, Fujiwara T, Sugiyama H, Yokoyama A, Takahashi H, Tanaka J. 2006. Molecular cloning and characterization of Nop25, a novel nucleolar RNA binding protein, highly conserved in vertebrate species. Exp Cell Res 312:1031–1041. https://doi.org/10.1016/j.yexcr.2005.12.017
44. Suzuki S, Fujiwara T, Kanno M. 2007. Nucleolar protein Nop25 is involved in nucleolar architecture. Biochem Biophys Res Commun 358:1114–1119. https://doi.org/10.1016/j.bbrc.2007.05.069
45. Oeffinger M, Zenklusen D, Ferguson A, Wei KE, El Hage A, Tollervey D, Chait BT, Singer RH, Rout MP. 2009. Rrp17p is a eukaryotic exonuclease required for 5' end processing of Pre-60S ribosomal RNA. Mol Cell 36:768–781. https://doi.org/10.1016/j.molcel.2009.11.011
46. Scott DD, Trahan C, Zindy PJ, Aguilar LC, Delubac MY, Van Nostrand EL, Adivarahan S, Wei KE, Yeo GW, Zenklusen D, Oeffinger M. 2017. Nol12 is a multifunctional RNA binding protein at the nexus of RNA and DNA metabolism. Nucleic Acids Res 45:12509–12528. https://doi.org/10.1093/nar/gkx963
47. Schneider CA, Rasband WS, Eliceiri KW. 2012. NIH image to ImageJ: 25 years of image analysis. Nat Methods 9:671–675. https://doi.org/10.1038/nmeth.2089
48. Bolte S, Cordelières FP. 2006. A guided tour into subcellular colocalization analysis in light microscopy. J Microsc 224:213–232. https://doi.org/10.1111/j.1365-2818.2006.01706.x
49. Ovesný M, Křížek P, Borkovec J, Svindrych Z, Hagen GM. 2014. ThunderSTORM: a comprehensive ImageJ plug-in for PALM and STORM data analysis and super-resolution imaging. Bioinformatics 30:2389–2390. https://doi.org/10.1093/bioinformatics/btu202
50. Clamme J-P, Krishnamoorthy G, Mély Y. 2003. Intracellular dynamics of the gene delivery vehicle polyethylenimine during transfection: investigation by two-photon fluorescence correlation spectroscopy. Biochim Biophys Acta 1617:52–61. https://doi.org/10.1016/j.bbamem.2003.09.002
51. Azoulay J, Clamme JP, Darlix JL, Roques BP, Mély Y. 2003. Destabilization of the HIV-1 complementary sequence of TAR by the nucleocapsid protein through activation of conformational fluctuations. J Mol Biol 326:691–700. https://doi.org/10.1016/s0022-2836(02)01430-4
52. Boisvert F-M, van Koningsbruggen S, Navascués J, Lamond AI. 2007. The multifunctional nucleolus. Nat Rev Mol Cell Biol 8:574–585. https://doi.org/10.1038/nrm2184
53. Glushonkov O, Réal E, Boutant E, Mély Y, Didier P. 2018. Optimized protocol for combined PALM-dSTORM imaging. Sci Rep 8:8749. https://doi.org/10.1038/s41598-018-27059-z
54. Bastiaens PI, Squire A. 1999. Fluorescence lifetime imaging microscopy: spatial resolution of biochemical processes in the cell. Trends Cell Biol 9:48–52. https://doi.org/10.1016/s0962-8924(98)01410-x
55. Voss TC, Demarco IA, Day RN. 2005. Quantitative imaging of protein interactions in the cell nucleus. Biotechniques 38:413–424. https://doi.org/10.2144/05383RV01
56. El Meshri SE, Dujardin D, Godet J, Richert L, Boudier C, Darlix JL, Didier P, Mély Y, de Rocquigny H. 2015. Role of the nucleocapsid domain in HIV-1 Gag oligomerization and trafficking to the plasma membrane: a fluorescence lifetime imaging microscopy investigation. J Mol Biol 427:1480–1494. https://doi.org/10.1016/j.jmb.2015.01.015
57. Ono A, Freed EO. 1999. Binding of human immunodeficiency virus type 1 Gag to membrane: role of the matrix amino terminus. J Virol 73:4136–4144. https://doi.org/10.1128/JVI.73.5.4136-4144.1999
58. Göttlinger HG, Sodroski JG, Haseltine WA. 1989. Role of capsid precursor processing and myristoylation in morphogenesis and infectivity of human immunodeficiency virus type 1. Proc Natl Acad Sci U S A 86:5781–5785. https://doi.org/10.1073/pnas.86.15.5781

59. Hermida-Matsumoto L, Resh MD. 2000. Localization of human immunodeficiency virus type 1 Gag and Env at the plasma membrane by confocal imaging. J Virol 74:8670–8679. https://doi.org/10.1128/jvi.74.18.8670-8679.2000
60. Guo J, Wu T, Anderson J, Kane BF, Johnson DG, Gorelick RJ, Henderson LE, Levin JG. 2000. Zinc finger structures in the human immunodeficiency virus type 1 nucleocapsid protein facilitate efficient minus- and plus-strand transfer. J Virol 74:8980–8988. https://doi.org/10.1128/jvi.74.19.8980-8988.2000
61. Dorfman T, Luban J, Goff SP, Haseltine WA, Göttlinger HG. 1993. Mapping of functionally important residues of a cysteine-histidine box in the human immunodeficiency virus type 1 nucleocapsid protein. J Virol 67:6159–6169. https://doi.org/10.1128/JVI.67.10.6159-6169.1993
62. Kafaie J, Song R, Abrahamyan L, Mouland AJ, Laughrea M. 2008. Mapping of nucleocapsid residues important for HIV-1 genomic RNA dimerization and packaging. Virology 375:592–610. https://doi.org/10.1016/j.virol.2008.02.001
63. Poon DT, Wu J, Aldovini A. 1996. Charged amino acid residues of human immunodeficiency virus type 1 nucleocapsid P7 protein involved in RNA packaging and infectivity. J Virol 70:6607–6616. https://doi.org/10.1128/JVI.70.10.6607-6616.1996
64. Schmalzbauer E, Strack B, Dannull J, Guehmann S, Moelling K. 1996. Mutations of basic amino acids of NCp7 of human immunodeficiency virus type 1 affect RNA binding *in vitro*. J Virol 70:771–777. https://doi.org/10.1128/JVI.70.2.771-777.1996
65. Mouhand A, Pasi M, Catala M, Zargarian L, Belfetmi A, Barraud P, Mauffret O, Tisné C. 2020. Overview of the nucleic-acid binding properties of the HIV-1 nucleocapsid protein in its different maturation states. Viruses 12:1109. https://doi.org/10.3390/v12101109
66. Cimarelli A, Sandin S, Höglund S, Luban J. 2000. Basic residues in human immunodeficiency virus type 1 nucleocapsid promote virion assembly via interaction with RNA. J Virol 74:3046–3057. https://doi.org/10.1128/jvi.74.7.3046-3057.2000
67. Dharan A, Bachmann N, Talley S, Zwikelmaier V, Campbell EM. 2020. Nuclear pore blockade reveals that HIV-1 completes reverse transcription and uncoating in the nucleus. Nat Microbiol 5:1088–1095. https://doi.org/10.1038/s41564-020-0735-8
68. Cimarelli A, Darlix J-L. 2002. Biomedicine and diseases: review¶assembling the human immunodeficiency virus type 1. Cell Mol Life Sci CMLS59:1166–1184. https://doi.org/10.1007/s00018-002-8495-6
69. Frankel AD, Young JA. 1998. HIV-1: fifteen proteins and an RNA. Annu Rev Biochem 67:1–25. https://doi.org/10.1146/annurev.biochem.67.1.1
70. Wilk T, Fuller SD. 1999. Towards the structure of the human immunodeficiency virus: divide and conquer. Curr Opin Struct Biol 9:231–243. https://doi.org/10.1016/S0959-440X(99)80033-5
71. Turner BG, Summers MF. 1999. Structural biology of HIV. J Mol Biol 285:1–32. https://doi.org/10.1006/jmbi.1998.2354
72. Briggs JAG, Simon MN, Gross I, Kräusslich H-G, Fuller SD, Vogt VM, Johnson MC. 2004. The stoichiometry of Gag protein in HIV-1. Nat Struct Mol Biol 11:672–675. https://doi.org/10.1038/nsmb785
73. Weeks SE, Metge BJ, Samant RS. 2019. The nucleolus: a central response hub for the stressors that drive cancer progression. Cell Mol Life Sci 76:4511–4524. https://doi.org/10.1007/s00018-019-03231-0
74. Pederson T. 2011. The nucleolus. Cold Spring Harb Perspect Biol 3:a000638. https://doi.org/10.1101/cshperspect.a000638
75. Jacobson MR, Pederson T. 1998. Localization of signal recognition particle RNA in the nucleolus of mammalian cells. Proc Natl Acad Sci U S A 95:7981–7986. https://doi.org/10.1073/pnas.95.14.7981
76. Pirogov SA, Gvozdev VA, Klenov MS. 2019. Long noncoding RNAs and stress response in the nucleolus. Cells 8:668. https://doi.org/10.3390/cells8070668
77. Thomson E, Ferreira-Cerca S, Hurt E. 2013. Eukaryotic ribosome biogenesis at a glance. J Cell Sci 126:4815–4821. https://doi.org/10.1242/jcs.111948
78. Sloan KE, Mattijssen S, Lebaron S, Tollervey D, Pruijn GJM, Watkins NJ. 2013. Both endonucleolytic and exonucleolytic cleavage mediate ITS1 removal during human ribosomal RNA processing. J Cell Biol 200:577–588. https://doi.org/10.1083/jcb.201207131
79. Kleinman CL, Doria M, Orecchini E, Giuliani E, Galardi S, De Jay N, Michienzi A. 2014. HIV-1 infection causes a down-regulation of genes involved in ribosome biogenesis. PLoS One 9:e113908. https://doi.org/10.1371/journal.pone.0113908
80. Boeras I, Song Z, Moran A, Franklin J, Brown WC, Johnson M, Boris-Lawrie K, Heng X. 2016. DHX9/RHA binding to the PBS-segment of the genomic RNA during HIV-1 assembly bolsters virion infectivity. J Mol Biol 428:2418–2429. https://doi.org/10.1016/j.jmb.2016.04.011
81. Brady S, Singh G, Bolinger C, Song Z, Boeras I, Weng K, Trent B, Brown WC, Singh K, Boris-Lawrie K, Heng X. 2019. Virion-associated, host-derived DHX9/RNA helicase A enhances the processivity of HIV-1 reverse transcriptase on genomic RNA. J Biol Chem 294:11473–11485. https://doi.org/10.1074/jbc.RA119.007679
82. Williams MC, Gorelick RJ, Musier-Forsyth K. 2002. Specific zinc-finger architecture required for HIV-1 nucleocapsid protein's nucleic acid chaperone function. Proc Natl Acad Sci U S A 99:8614–8619. https://doi.org/10.1073/pnas.132128999
83. Kankia BI, Barany G, Musier-Forsyth K. 2005. Unfolding of DNA quadruplexes induced by HIV-1 nucleocapsid protein. Nucleic Acids Res 33:4395–4403. https://doi.org/10.1093/nar/gki741
84. Rajendran A, Endo M, Hidaka K, Tran PLT, Mergny J-L, Gorelick RJ, Sugiyama H. 2013. HIV-1 nucleocapsid proteins as molecular chaperones for tetramolecular antiparallel G-quadruplex formation. J Am Chem Soc 135:18575–18585. https://doi.org/10.1021/ja409085j
85. Butovskaya E, Soldà P, Scalabrin M, Nadai M, Richter SN. 2019. HIV-1 nucleocapsid protein unfolds stable RNA G-quadruplexes in the viral genome and is inhibited by G-quadruplex ligands. ACS Infect Dis 5:2127–2135. https://doi.org/10.1021/acsinfecdis.9b00272
86. Jain A, Bacolla A, Del Mundo IM, Zhao J, Wang G, Vasquez KM. 2013. DHX9 helicase is involved in preventing genomic instability induced by alternatively structured DNA in human cells. Nucleic Acids Res 41:10345–10357. https://doi.org/10.1093/nar/gkt804
87. Chakraborty P, Grosse F. 2011. Human DHX9 helicase preferentially unwinds RNA-containing displacement loops (R-loops) and G-quadruplexes. DNA Repair (Amst) 10:654–665. https://doi.org/10.1016/j.dnarep.2011.04.013
88. Lee T, Pelletier J. 2016. The biology of DHX9 and its potential as a therapeutic target. Oncotarget 7:42716–42739. https://doi.org/10.18632/oncotarget.8446
89. Mekdad HE, Boutant E, Karnib H, Biedma ME, Sharma KK, Malytska I, Laumond G, Roy M, Réal E, Paillart J-C, Moog C, Darlix JL, Mély Y, de Rocquigny H. 2016. Characterization of the interaction between the HIV-1 Gag structural polyprotein and the cellular ribosomal protein L7 and its implication in viral nucleic acid remodeling. Retrovirology 13:54. https://doi.org/10.1186/s12977-016-0287-4